CHAPTER 4

RESULT AND DISCUSSION

In this chapter a detailed analysis of the data collected from experimentation was conducted and discussed. Data gathered from the experimental setup was interpreted to evaluate various parameters, which affect the indoor thermal behavior of the building. Section 4.1 contains results and discussion on short duration analysis field testing. In section 4.2, analysis on various parameters of long duration (Yearly analysis) field testing was presented. Section 4.3 discussed about thermal characterization of the PCM.

4.1 Short duration analysis (24 hour)

4.1.1 Indoor temperature profile

The indoor thermal behavior of both the cubicles was recorded for 24 hours on 12th July 2018 and is analyzed in terms of indoor temperature, thermal amplitude and time lag. Figures 4.1 – 4.6 shows the variation in the temperature profile of the south wall, west wall, north wall, east wall, the roof, and the indoor ambient respectively, of the reference and experimental cubicle for the 24 hours on 12th July 2018. The outside ambient air temperature of the 12th of July is also shown in the figures. All the four walls of the cubicles exhibit, more or less, the same temperature profile trend for 24 hours. The inside surface temperature of the experimental cubicle walls remains below during the day in comparison to the reference cubicle walls. This is because of the presence of macroencapsulated PCM in the walls of the experimental cubicle. The amount of increase in the incident solar radiation on the walls of experimental cubicle will cause the temperature to rise and consequently, the PCM starts melting and stores thermal energy in the latent form. During the night, the inside

surface temperature of all the walls of experimental cubicle remains higher in comparison to the temperature of reference cubicle walls. This is because of the fact that PCM discharges and releases its latent heat to the surrounding when ambient air temperature starts falling because of the reduced or no incident solar radiation. This can be correlated with the solid-liquid and liquid-solid phase transition of the PCM. The released heat, during the solidification of the PCM, will increase the indoor ambient temperature to an uncomfortable thermal range if it is not handled carefully. Therefore, there must be some ventilation arrangement in the building like windows, ventilators, exhaust system, and etc. to dissipate this liberated heat to the atmosphere.

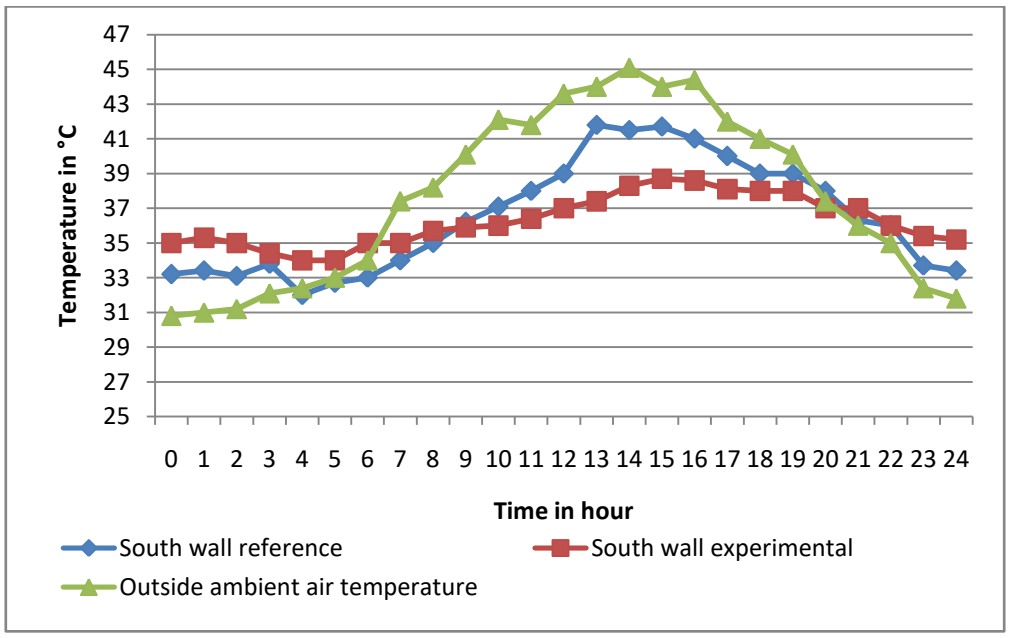

Figure 4.1 South wall temperatures of reference and experimental cubicle on 12th July 2018

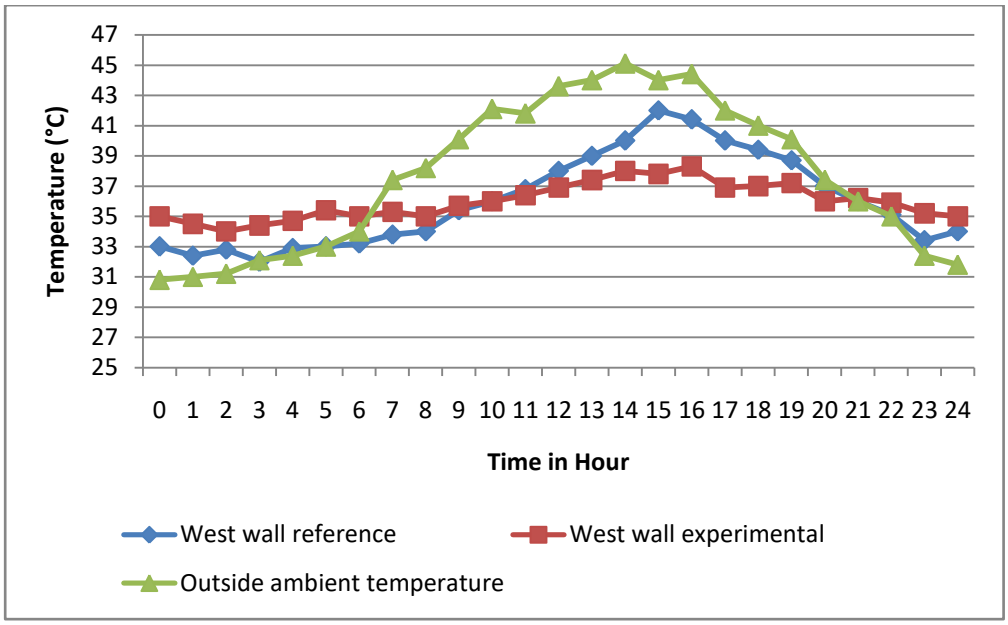

Figure 4.2 West wall temperature of reference and experimental cubicle on 12th July 2018

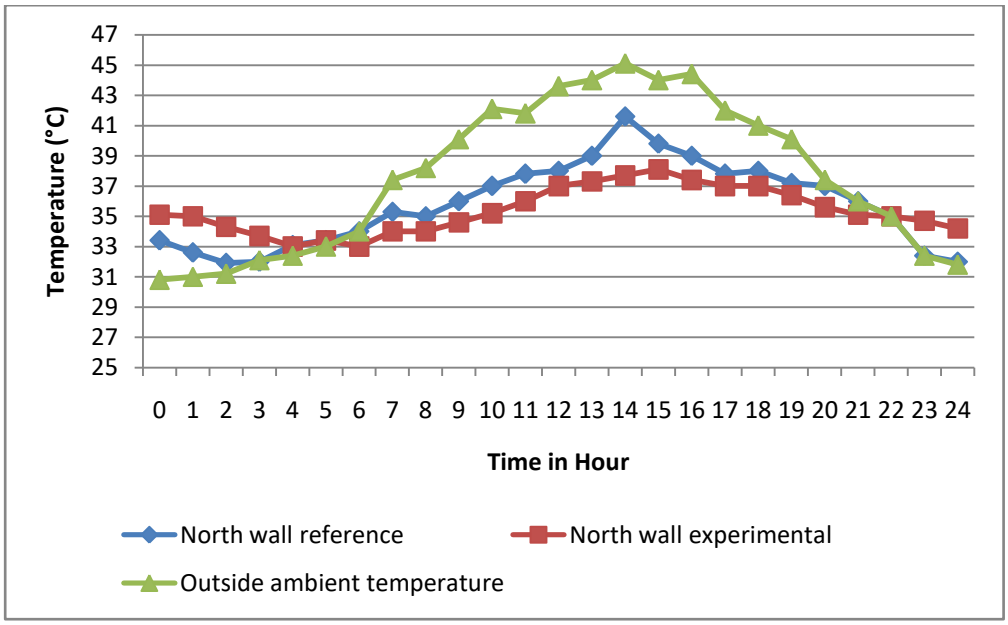

Figure 4.3 North wall temperature of reference and experimental cubicle on 12th July 2018

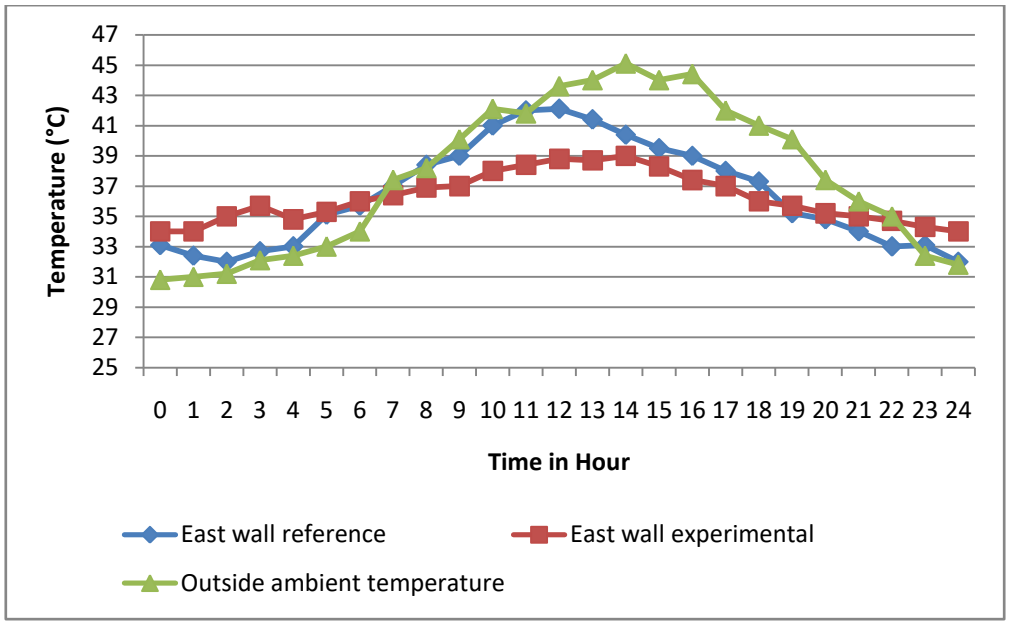

Figure 4.4 East wall temperature of reference and experimental cubicle on 12th July 2018

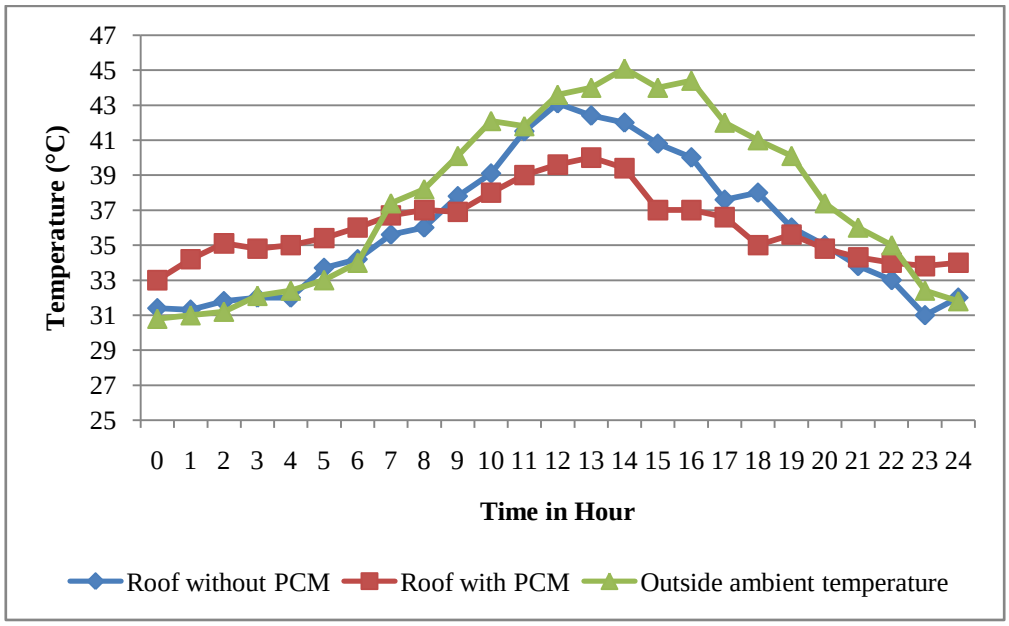

Figure 4.5 Roof temperatures of reference and experimental cubicle on 12th July 2018

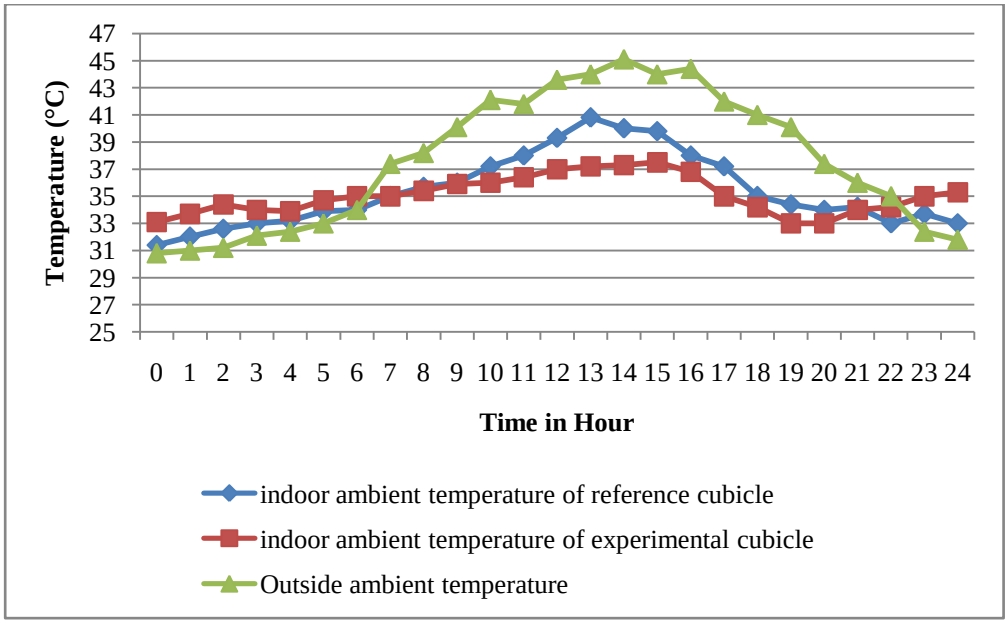

Figure 4.6 Indoor ambient temperatures of reference and experimental cubicle on 12th July 2018

Table 4.1 shows the comparative analysis of reference and experimental cubicle walls, roofs, and indoor ambient temperatures. The south, west, north and east walls of reference cubicle attain maximum temperature mark of 41.8°C, 42.0°C, 41.6°C and 42.1°C respectively. Whereas, the walls of experimental cubicle shows a lower temperature profile and attains 38.7°C, 38.3°C, 38.1°C and 39.0°C for south, west, north and east walls respectively. The roof and indoor ambient temperature of the reference cubicle are 43.1°C and 40.8°C respectively, whereas the experimental cubicle roof and indoor ambient temperature are 40.0°C and 38.0°C respectively. A percentage reduction of 7.41%, 8.80%, 9.18%, 7.36%, 7.19% and 8.08% in peak temperature of the experimental cubicle south wall, west wall, north wall, east wall, roof and inside ambient respectively was achieved in comparison to the reference cubicle walls, roof and inside ambient.

Table 4.1 Comparison of peak temperature of reference cubicle and experimental cubicle walls

Orientation	**T_{peak} (Reference) (°C)**	**T_{peak} (Experimental) (°C)**	**ΔT_{peak} (Peak temperature difference) (°C)**	**Reduction in peak temperature in %**
South wall	41.8	38.7	3.1	7.41
West wall	42.0	38.3	3.7	8.80
North wall	41.6	38.1	3.5	9.18
East wall	42.1	39.0	3.1	7.36
Roof	43.1	40	3.1	7.19
Indoor ambient	40.8	37.5	3.3	8.08

The thermal amplitude of the building is the measure of the daily maximum and minimum temperature. It is important to minimize the thermal amplitude of the building envelope for better thermal stability and also to improve the thermal response. Table 4.2 indicates the variation in thermal amplitude of both the cubicles and the percentage reduction in thermal amplitude (α) achieved by the experimental cubicle. The reduction in α, ranging from 40.67 % to 59.79 % is achieved by the walls of the experimental cubicle. The roof of the experimental cubicle shows a minimum % reduction of 40.67 %, whereas the north wall of the experimental cubicle shows a maximum reduction of 59.79 %. Among the four walls, the least percentage reduction in thermal amplitude is shown by the east wall (α=50.40%). The order of the percentage reduction of the thermal amplitude for all the orientations is $\alpha_{north} > \alpha_{south} > \alpha_{west} > \alpha_{ambient} > \alpha_{east} > \alpha_{roof}$. Least value of α indicates that the percentage reduction in temperature swing is minimum. Large value of α indicates percentage reduction temperature swing is maximum. Therefore, this result indicates that the orientation with the

least value of α must be integrated with a large quantity of the PCM to reduce the indoor temperature fluctuations effectively.

Table 4.2 Comparison of thermal amplitude of reference and experiment cubicle

Orientation	**Reference cubicle**		**Experimental cubicle**		**(ΔT_r) Thermal amplitude of reference cubicle ($T_{max,r}$- $T_{min,r}$)**	**(ΔT_e) Thermal amplitude of experimental cubicle ($T_{max,e}$- $T_{min,e}$)**	**(α) %Reduction in thermal amplitude (ΔT_r- ΔT_e)/ ΔT_r %**
	$T_{max,r}$	**$T_{min,r}$**	**$T_{max,e}$**	**$T_{min,e}$**			
South	41.8	33.1	38.7	35.0	8.7	3.7	57.47 %
West	42.0	32.0	38.3	34.0	10	4.3	57.0 %
North	41.6	31.9	38.1	34.2	9.7	3.9	59.79 %
East	42.1	32.0	39.0	34.0	10.1	5.0	50.40 %
Roof	43.1	31.3	40	33.0	11.8	7.0	40.67 %
Inside ambient	40.8	31.4	37.5	33.1	9.4	4.4	53.19 %

Another factor that plays an important role in maintaining the indoor thermal comfort is the time lag (Φ). Time lag is the time delay in achieving the peak temperature mark. This effect is particularly important in the design of the buildings in an environment with a high diurnal range. In some places, for example in deserts, the daytime temperature reaches the mark of 40-45˚C. The following night, however, the temperature can fall below the freezing range. In such places, the utilization of the appliances (fan, cooler and air-conditioner) will increase in order to keep the temperature under normal condition. Therefore, an increase in time delay will reduce the dependency on the appliances used for space cooling and heating. Figure 4.7 shows the time lag achieved by the experimental cubicle in comparison to the reference cubicle. A maximum of 120 minutes of time lag was achieved by the south wall, east wall and indoor ambient temperature. West wall, north wall,

and the roof attained a time lag of 60 minutes each. This time lag will remarkably reduce the cooling load of the building envelope by reducing the usage of electrical appliances for space cooling for at least 60 to 120 minutes inside the building. Moreover, this will also help in proving the concept of cooling load shifting.

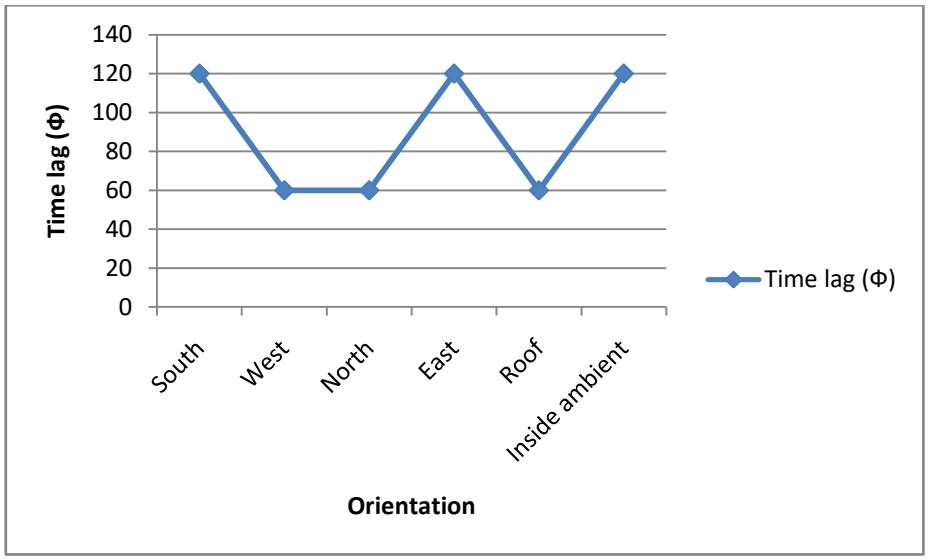

Figure 4.7 Time lag of experimental cubicle compared to the reference cubicle

4.1.2 Heat flux and cooling load reduction

Heat flux sensors were used to measure the quantity of the heat flow through the walls and roofs of both the cubicles. Figure 4.8 (a) - (e) shows the measured heat flux across the south wall, west wall, north wall, east wall and the roof of reference and experimental cubicle on 12th July 2018. The analysis of the graphs suggests that the heat flux of the experimental cubicle walls was lower than those of reference cubicle walls before reaching to their respective peak. After reaching the peak, the heat flux of experimental walls is comparable or slightly higher than the reference cubicle walls. This trend is because of the phase transition of PCM from solid-liquid, before reaching the peak, and liquid to solid after reaching the peak. The area of the graph lying below the reference cubicle line and above

the experimental cubicle line will be equal to the amount of heat stored by the MPCM during the solid-liquid phase transition. Whereas, the area lying below the experimental cubicle line and above reference cubicle is the amount of heat discharged by the PCM during the liquid-solid phase transition.

The orientation, which shows the minimum amount of heat transfer due to the presence of MPCM was the roof, followed by the south wall, east wall, west wall and the north wall of the experimental cubicle. The peak heat flux of both the cubicles and corresponding percentage reduction is shown in the figure 4.9. A maximum of 41.31 % reduction was achieved by the east wall of the experimental cubicle followed by 31.69 %, 20.59 %, 20.19 % and 19.41 % by the west wall, north wall, south wall, and the roof respectively. The sum of the peak heat flux of all the orientations of the reference and the experimental cubicle was 78.29 W/m^2 and 56.896 W/m^2 respectively. Thus, a reduction of 27.32 % in total peak heat flux has been achieved by the experimental cubicle in comparison to the reference cubicle. The cooling load of the cubicles must be equal to the sum of the total heat flux of all the orientations if the radiation heat transfers between the internal surfaces of the walls were neglected. It is difficult to calculate the effect of each wall on the space cooling because of varying shape and orientation of the buildings. Therefore, to evaluate the cooling load of each cubicle all the fluxes of each wall were added.

Total cooling load of the reference cubicle = heat flux (east wall + west wall + north wall + south wall + roof) -------(1)

Total cooling load of the experimental cubicle = heat flux (east wall + west wall + north wall + south wall + roof) -------(2)

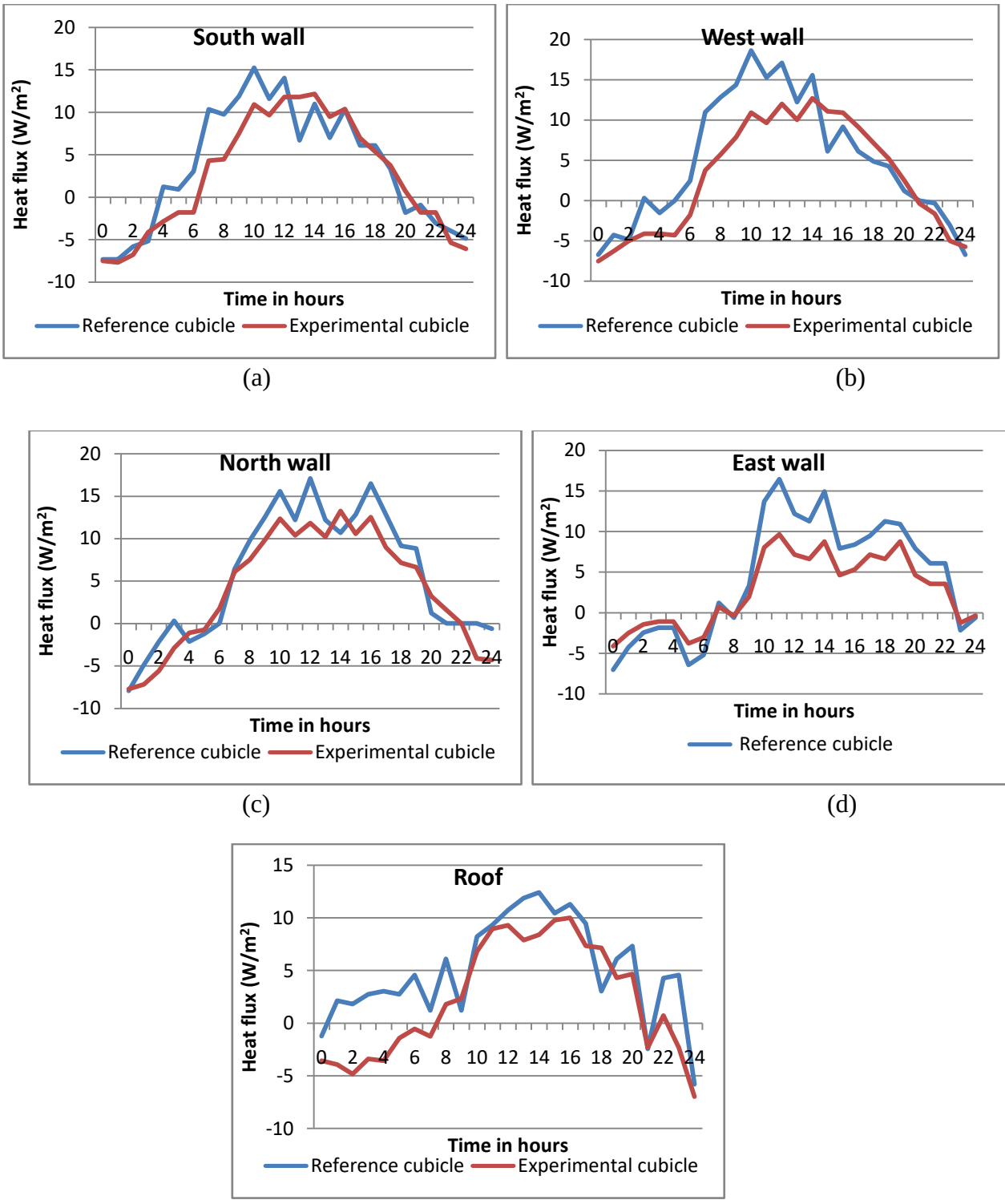

Figure 4.8 Heat flux across (a) South wall (b) West wall (c) North wall (d) East wall (e) Roof

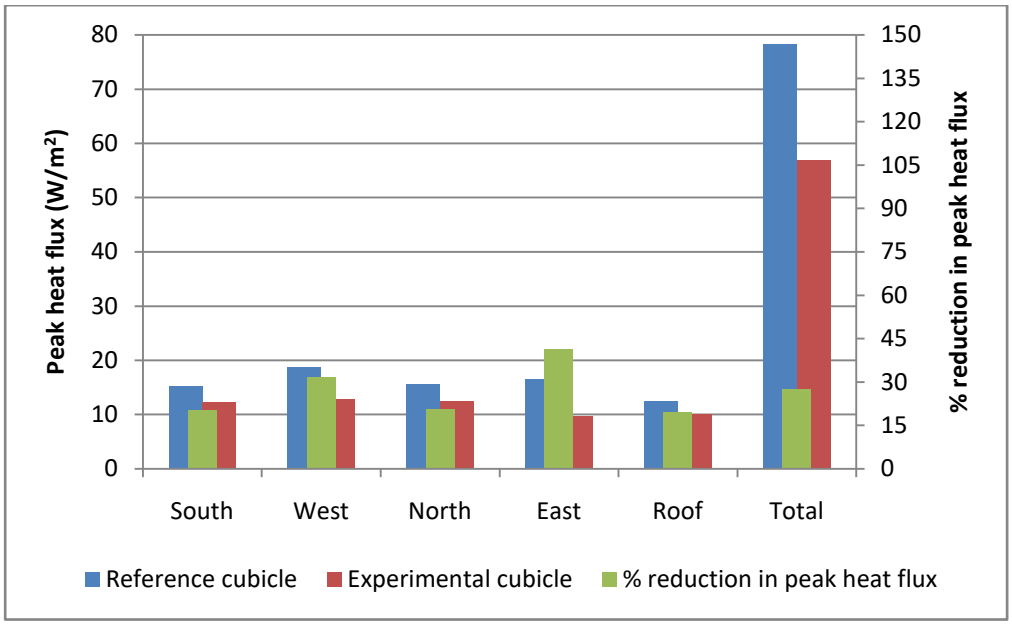

Figure 4.9 Peak heat flux and corresponding percentage reduction of both the cubicles

Now, from equation (1) and from equation (2) we can calculate the reduction in cooling load (108) i.e.

The reduction in cooling load = Total cooling load of the reference cubicle - Total cooling load of the experimental cubicle ------ --(3)

Putting the values in the equation (3), we get 226.99 watts of reduction in cooling load. Thus, using MPCM in the building walls, a reduction of 38.76 % in cooling load can be achieved.

To evaluate the cost savings in electricity consumption, the price of per kWh of electricity must be known. Considering the cost of electricity as 5.20 Rupees/kWh, as per the Central Electricity Authority of India.

Therefore, cost savings in electricity = reduction in cooling load (kW) × price of electricity (per kWh) × 24 hours

Thus, the cost saving of 28.31 Rupees/day (~0.40 US $/day) in electricity consumption is achieved in the experimental cubicle.

4.1.2 Thermal analysis using infrared thermography

Instead of analyzing the thermal response of the whole wall or a larger section of a wall, the thermocouples only evaluate the temperature variation of a particular point/location on the wall. There might be chances that the thermal behavior of one location/point on the wall differs from another location/point on the same wall at the same time. Therefore, to evaluate the thermal response of a larger section of the wall, the thermography analysis of the walls of the experimental and the reference cubicle has been done using an infrared thermographic camera named Testo-865 having thermal sensitivity of 120 mK purchased from Testo, Germany. The thermal images of the section of the wall obtained from thermography are then analyzed using PC analysis software called Testo IRsoft of version 4.3.3549.32851. To ensure that the exact value of the temperature is recorded, the material emissivity was obtained by direct comparison to a material with known emissivity. An emissivity of 0.95 was evaluated for all the specimens which are observed.

Figure 4.10 – 4.13 are the thermal images of the inside surface of the south wall obtained at 9:00 a.m., 12:00 p.m., 3:00 p.m. and, 6:00 p.m. respectively. These images show the inside surface thermal profile of south wall of both the cubicles and the temperature distribution, of the images captured, varies is as per the scale associated with each image. The highest temperature is represented by the red color and the lowest temperature is represented by the blue color. The average temperature of the south wall of the experimental cubicle is less than the average temperature of the south wall of the reference cubicle in all

the images. This is because of the absence of latent heat storage in reference cubicle, which leads to increase in average surface temperature at 9:00 a.m., 12:00 p.m., 3:00 p.m. and 6:00 p.m. Presence of macroencapsulated PCM in the walls of experimental cubicle increases its thermal storage capacity and hence the average temperature of the south wall is less.

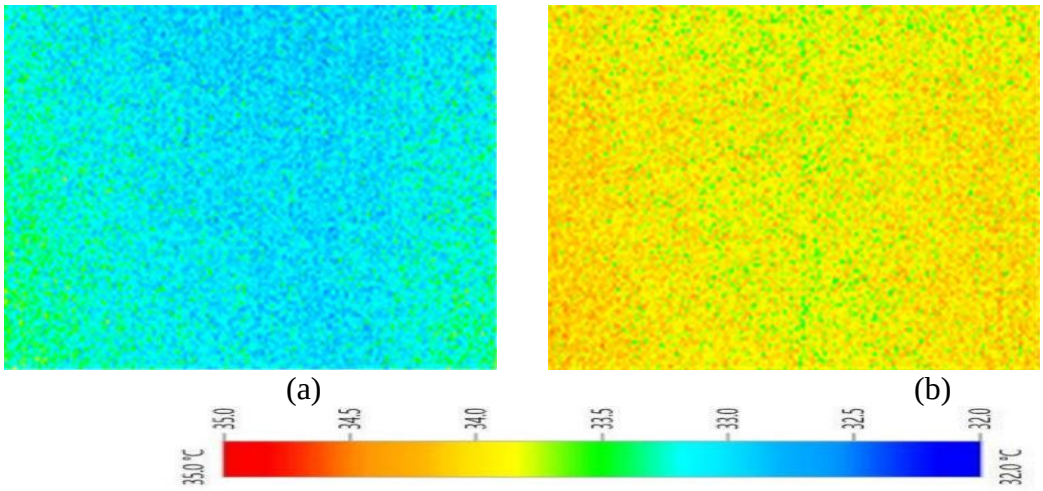

Figure 4.10 (a) Thermal image of South wall of experimental cubicle at 9:00 a.m. (b) Thermal image of South wall of reference cubicle at 09:00 a.m.

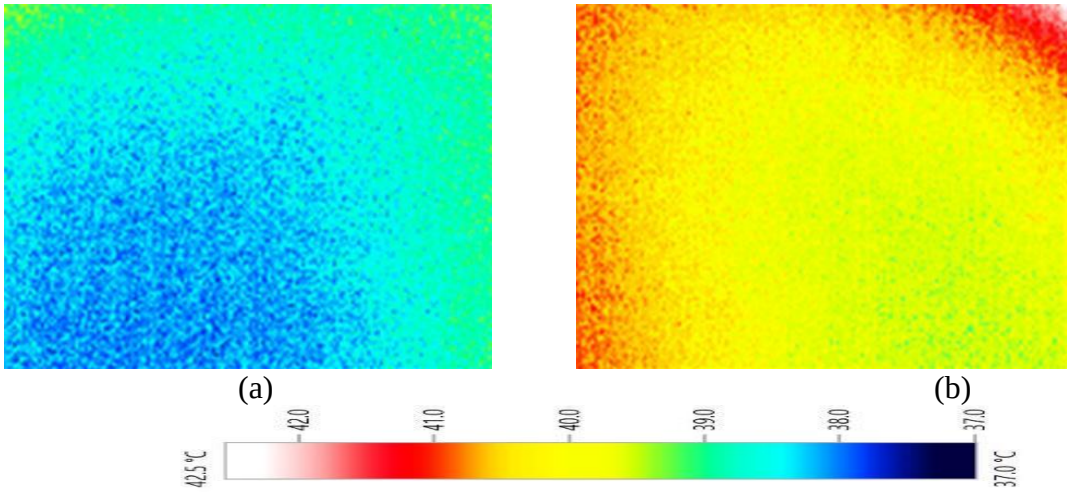

Figure 4.11 (a) Thermal image of South wall of experimental cubicle at 12:00 p.m. (b) Thermal image of South wall of reference cubicle at 12:00 p.m.

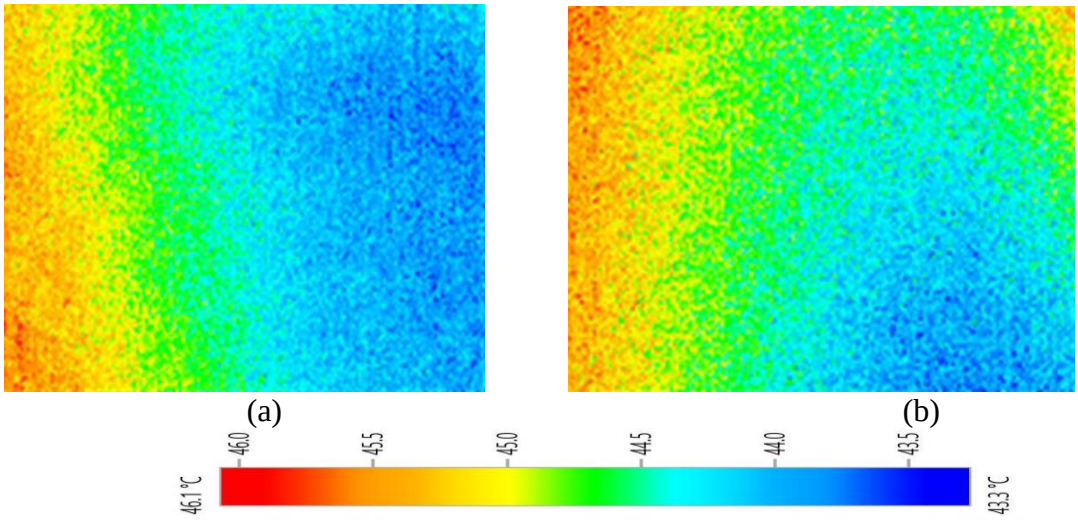

Figure 4.12 (a) Thermal image of South wall of experimental cubicle at 3:00 p.m. (b) Thermal image of South wall of reference cubicle at 3:00 p.m.

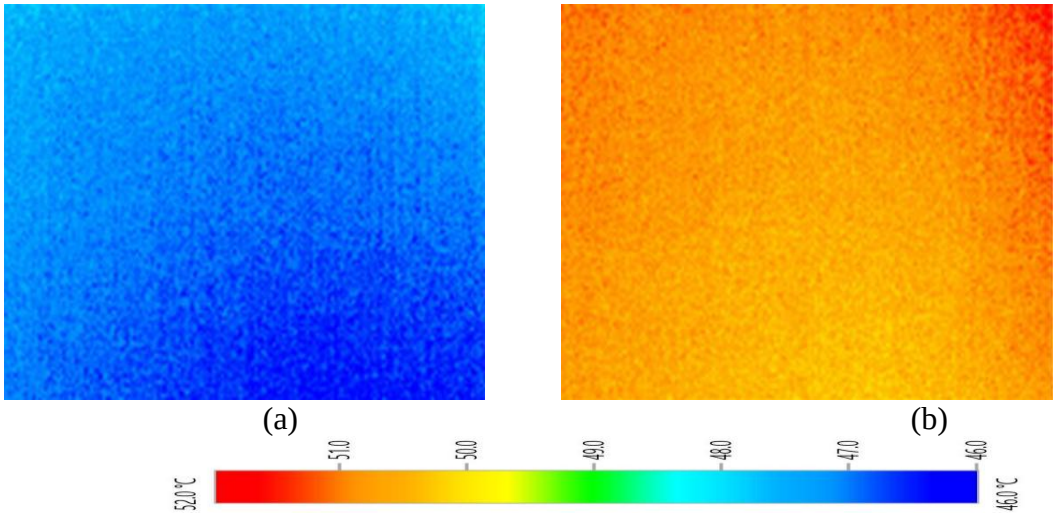

Figure 4.13 (a) Thermal image of South wall of experimental cubicle at 6:00 p.m. (b) Thermal image of South wall of reference cubicle at 6:00 p.m.

4.2 Long duration analysis (Yearly Analysis)

The main focus of this analysis is to analyze the indoor thermal behavior of the experimental cubicle with respect to the reference cubicle for different months/seasons of the year. In yearly analysis the investigation of all the factors affecting indoor thermal comfort was conducted by considering only indoor ambient temperature of both the cubicles. Therefore, the indoor ambient temperature of both the cubicles was recorded and is shown in Figure 4.14 – Figure 4.25. Along with the indoor temperature, the intensity of solar radiation during the testing period was also shown in figures. The recorded data shows a variation in the pattern of the indoor temperature of both the cubicles with time. This variation is because of the difference in the latent heat storage capacity of the cubicles.

4.2.1 Annual indoor temperature profile

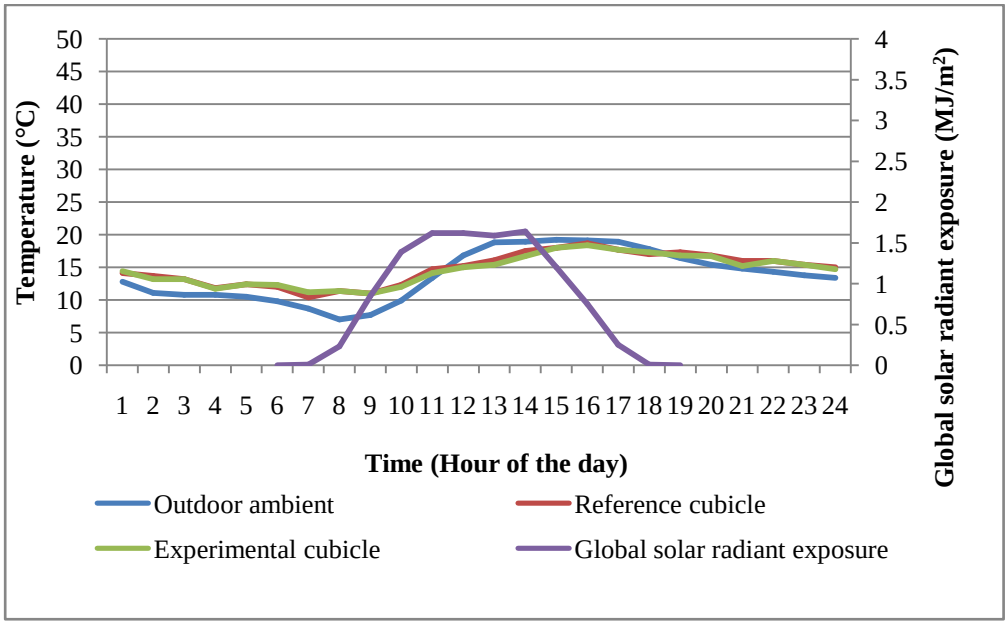

Figure 4.14 Temperature profile of 1st Jan 2019 of reference and experimental cubicle

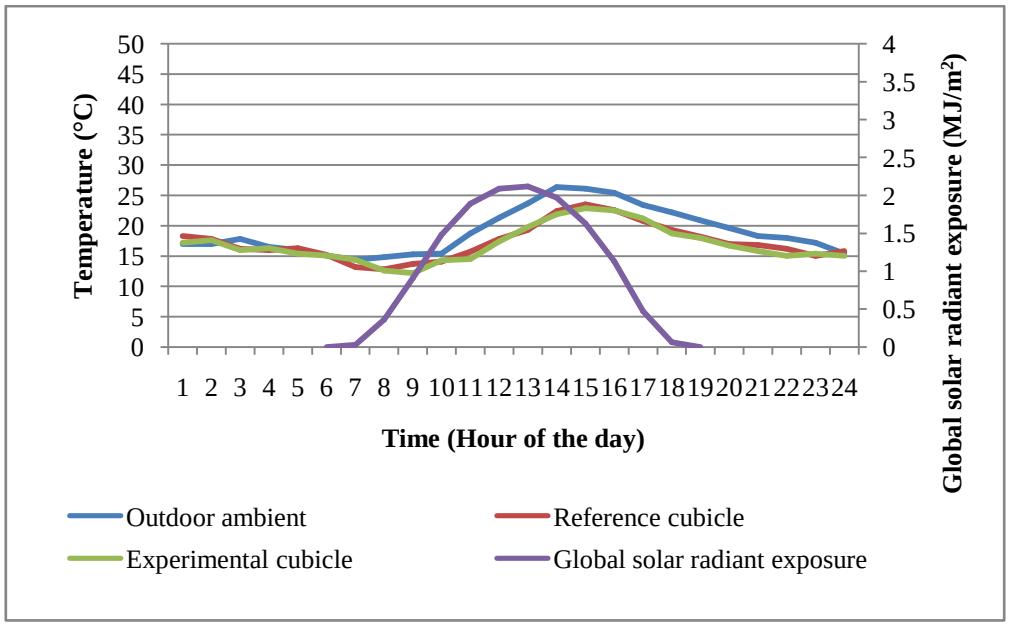

Figure 4.15 Temperature profile of 2nd February 2019 of reference and experimental cubicle

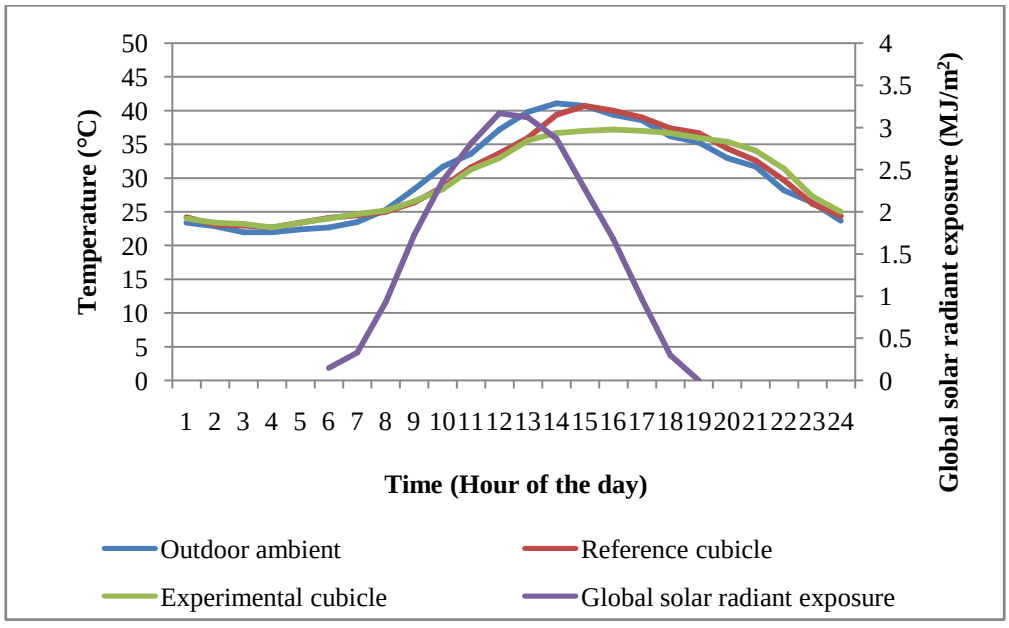

Figure 4.16 Temperature profile of 3rd March 2019 of reference and experimental cubicle

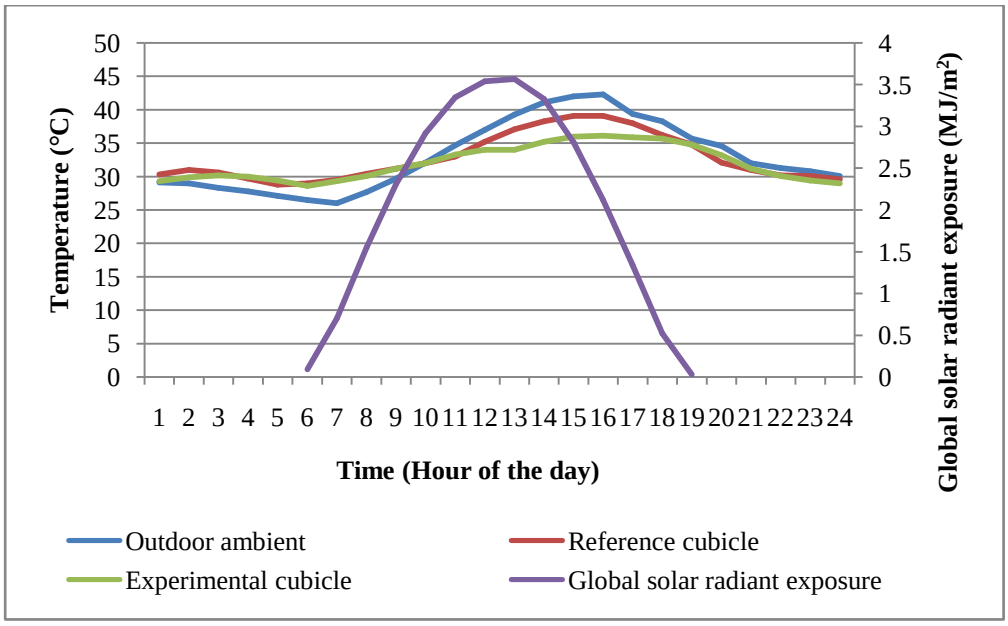

Figure 4.17 Temperature profile of 4th April 2019 of reference and experimental cubicle

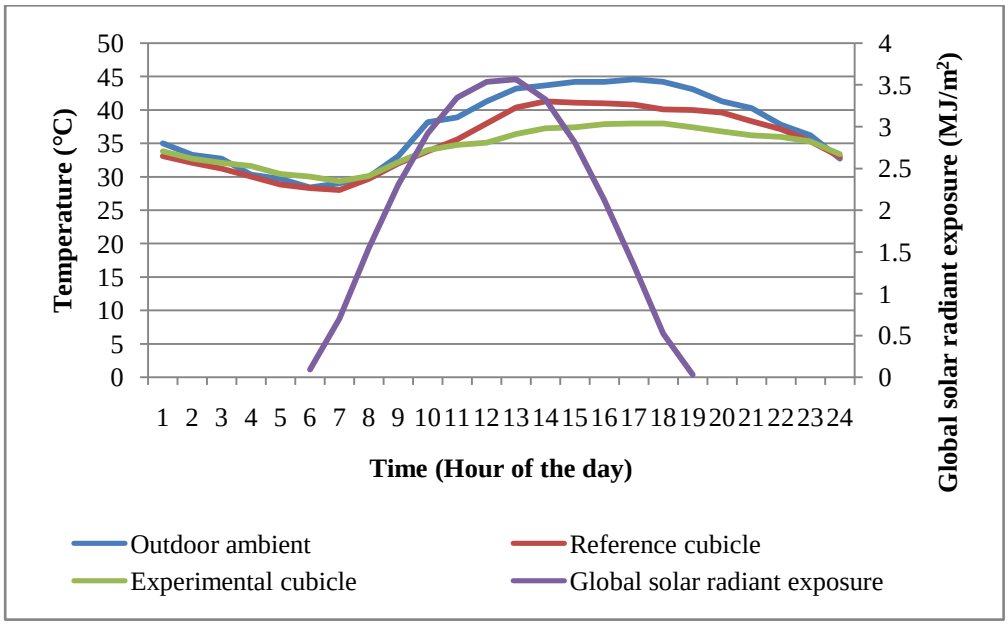

Figure 4.18 Temperature profile of 5th May 2019 of reference and experimental cubicle

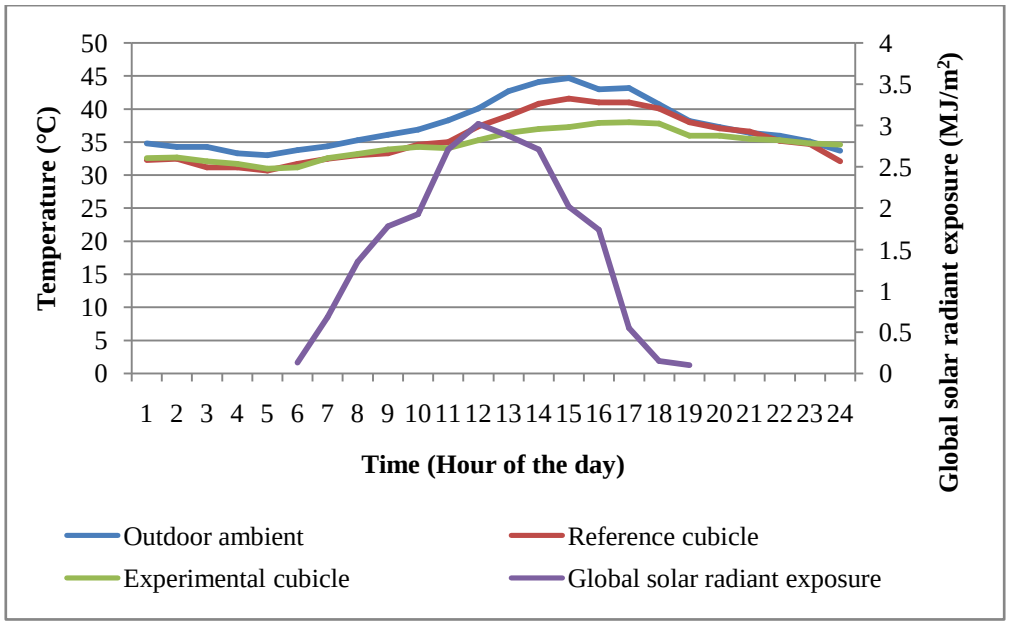

Figure 4.19 Temperature profile of 6th June 2019 of reference and experimental cubicle

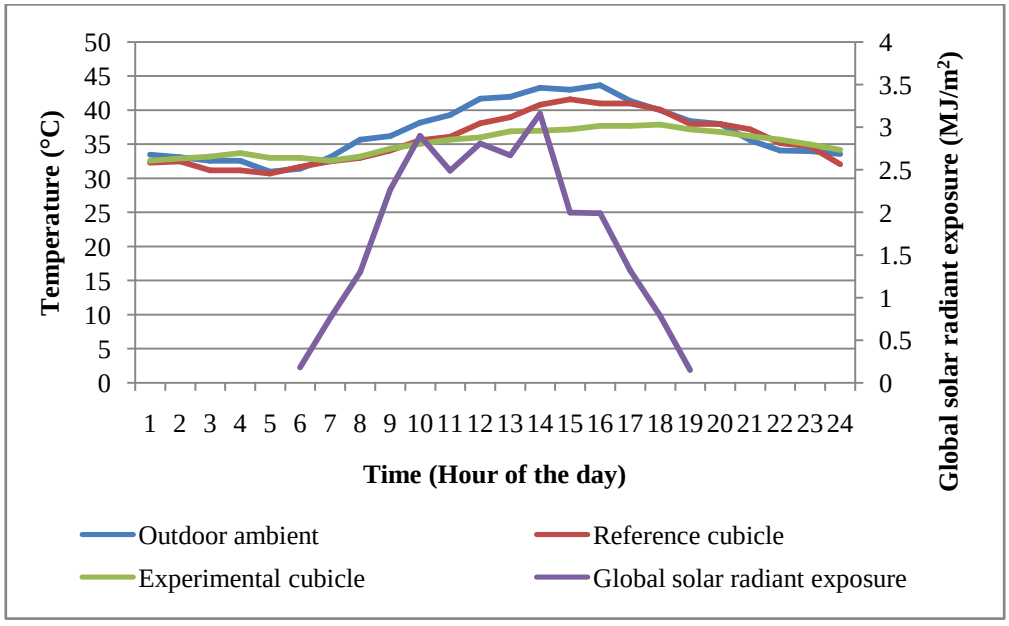

Figure 4.20 Temperature profile of 7th July 2019 of reference and experimental cubicle

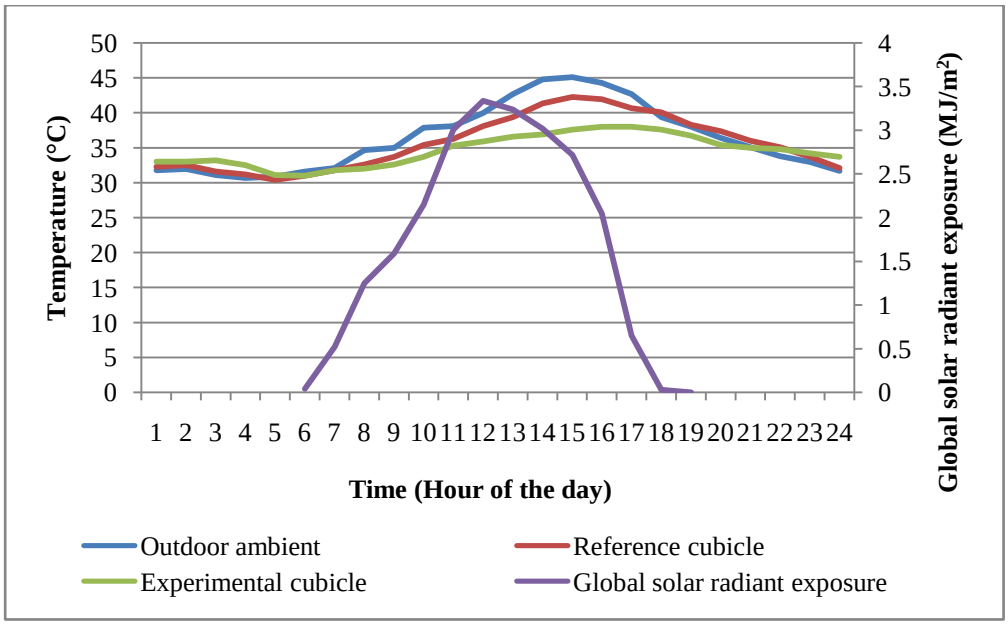

Figure 4.21 Temperature profile of 8th August 2019 of reference and experimental cubicle

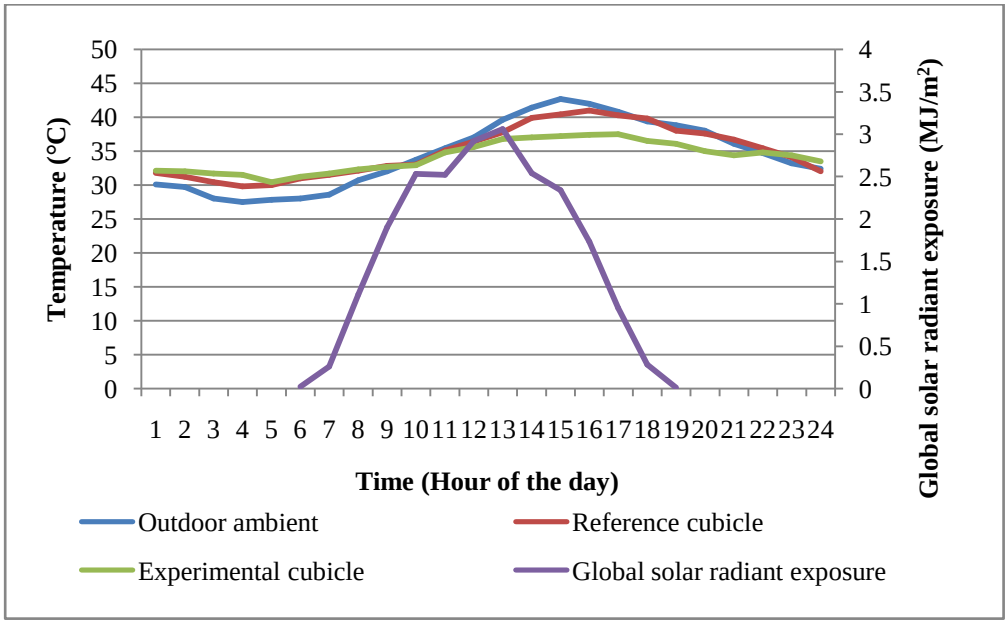

Figure 4.22 Temperature profile of 9th September 2019 of reference and experimental cubicle

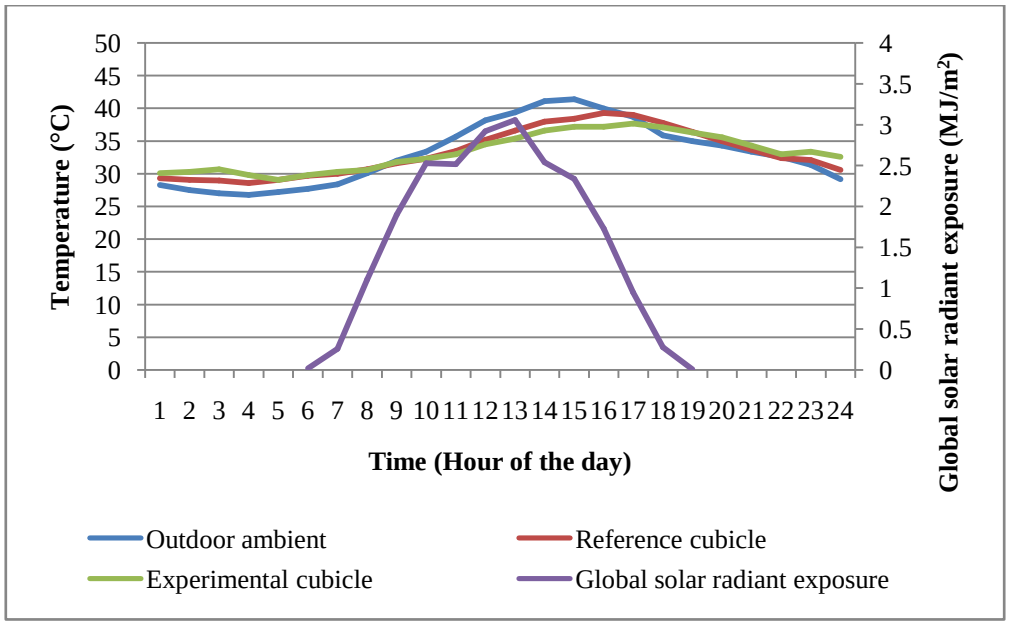

Figure 4.23 Temperature profile of 10th October 2019 of reference and experimental cubicle

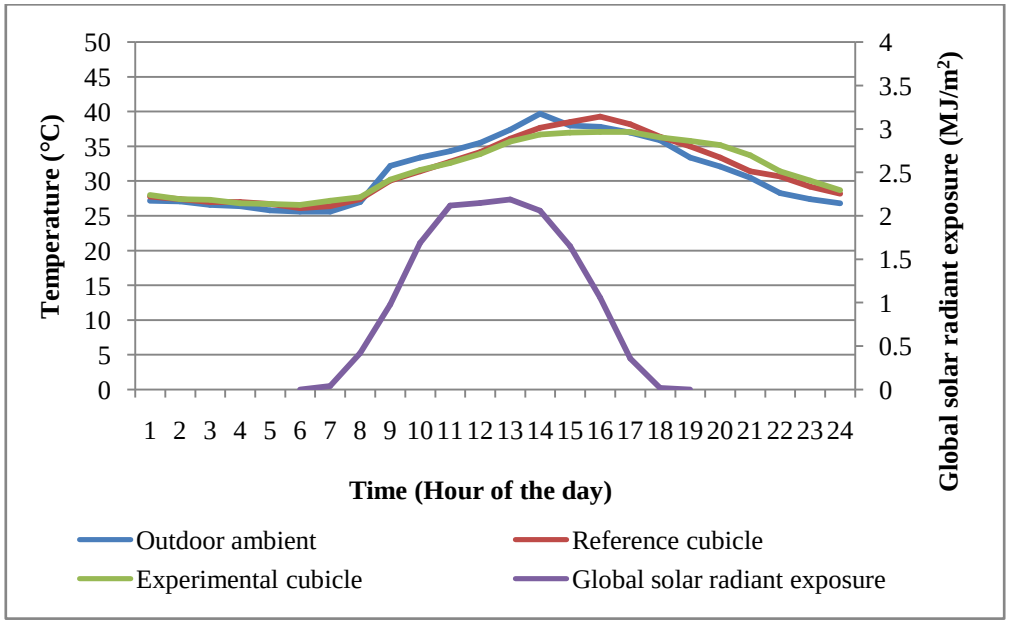

Figure 4.24 Temperature profile of 11th November 2019 of reference and experimental cubicle

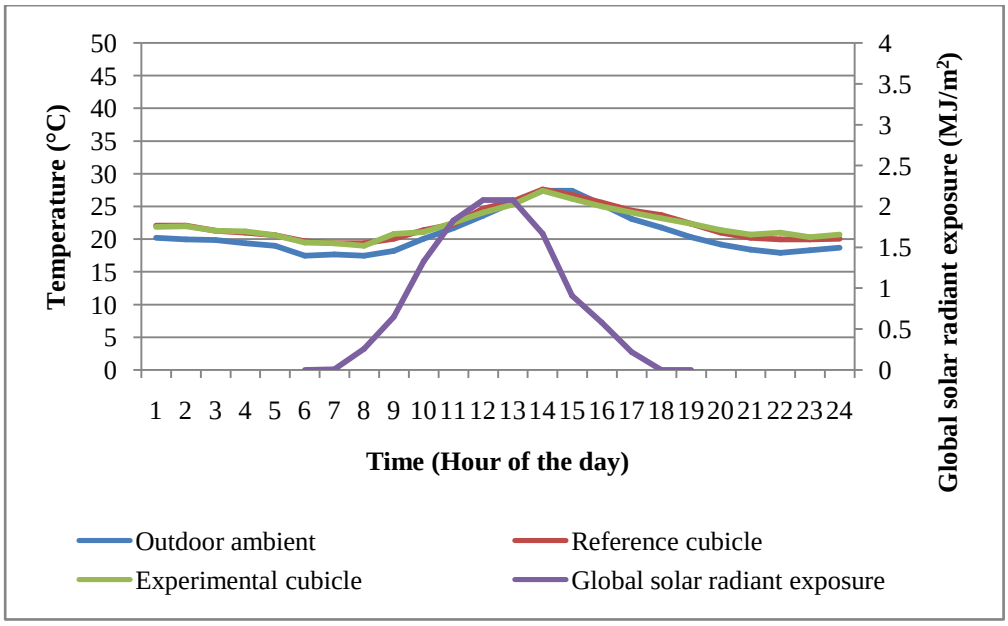

Figure 4.25 Temperature profile of 12th December 2019 of reference and experimental cubicle

An important factor that affects the cooling load of the buildings is the peak temperature. Peak temperature corresponds to the time of the day when the indoor temperature of the building envelope is maximum. This condition can increase the demand for cooling in the buildings, raising the energy expenditure. Analysis suggests that for each degree of increase in the temperature, the increase in the peak electricity load varies from 0.45% to 4.6%, which corresponds to an increase in electricity consumption of about 21 W per degree of temperature increase per person (279). Another study (280) revealed that an increase in the ambient air temperature by 5.9°C, the demand for cooling in the buildings will elevate by 23.5%. Additionally, an increase in the peak temperature may cause overheating of the building envelope and consequently leads to the formation of Urban Heat Island (UHI) (281,282). Therefore, to reduce the risk of overheating and the formation of UHI it is evident to reduce the indoor peak temperature mark of the building envelope to improve the thermal energy performance of the building. Furthermore, a reduction in peak

temperature will also reduce the energy demand for cooling. The analysis of the measured data shows that for all the months, the recorded daily peak temperature of the experimental cubicle remains low in comparison to the reference cubicle. Months of the winter season, i.e. January, February, and December, shows the least or almost negligible difference in the indoor daily peak temperature, whereas months of the summer season, i.e. March, April, May, June, July, August, and September shows the highest or major difference in the indoor daily peak temperature of the experimental cubicle in comparison to the reference cubicle. The highest difference of 4.3°C was recorded in August whereas the lowest difference of 0.2°C was obtained in December.

Table 4.3 Monthly peak temperature reduction of reference and experimental cubicle

S.No.	Month	Reference cubicle peak temperature (°C)	Experimental cubicle peak temperature (°C)	Peak temperature difference (°C)
1.	January	18.7	18.4	0.3
2.	February	23.5	22.9	0.6
3.	March	40.7	37.2	3.5
4.	April	39.1	36	3.1
5.	May	41.3	38	3.3
6.	June	41.6	38	3.6
7.	July	41.6	37.9	3.7
8.	August	42.3	38	4.3
9.	September	41	37.5	3.5
10.	October	39.3	37.7	1.6
11.	November	39.3	37.1	2.2
12.	December	27.6	27.4	0.2

Table 4.3 shows the details of the month-wise daily peak temperature of both the cubicles. These results suggest that the maximum utilization of the latent heat storage of the PCM, when embedded in the building envelope, is during the summer season/months. However, in the winter season, there is almost negligible variation in the indoor temperature

profile of both the cubicles. This is because of the fact that throughout the winter season the maximum peak temperature remains below the melting temperature range of the PCM (i.e. 36°C to 38°C) and because of this the PCM doesn't melt and consequently leads to no utilization of the latent heat of the PCM. In tropical countries, the diurnal temperature range is higher in comparison to the countries lying in the colder region. Increase in the diurnal temperature range increases the indoor temperature swing of the building and thus gives rise to thermal un-stability. Therefore, there is a need to reduce the daily fluctuations in the indoor temperature of the buildings as much as possible. Their evaluation becomes more important for the countries having hot climate to reduce the cooling load demand and to provide an comfortable indoor condition. Table 4.4 shows the comparison of the month-wise daily indoor thermal amplitude of reference and experimental cubicle. It has been analyzed that the months falling in the summer season recorded the maximum reduction in the indoor thermal amplitude of the experimental cubicle in comparison to the reference cubicle. However, the winter season has recorded the minimum reduction in the thermal amplitude. The month of July has shown a maximum percentage reduction of 51.37%, while December has experienced a negative percentage reduction of -2.43% in the thermal amplitude of the experimental cubicle in comparison to the reference cubicle. The order of the reduction in the thermal amplitude of each month of the year is: $\alpha_{july} > \alpha_{august} > \alpha_{september} > \alpha_{june} > \alpha_{may} > \alpha_{april} > \alpha_{march} > \alpha_{november} > \alpha_{january} > \alpha_{february} > \alpha_{december}$. These results suggest that the maximum utilization of the latent heat storage of the PCM is done during the summer season when the atmosphere is relatively hot and solar radiation is intense. However, in winter season, the atmospheric temperature remains below the transition temperature range of the PCM. Consequently, the PCM doesn't melt causing no utilization of the latent heat storage property of the MPCM.

Table 4.4 Comparison of the monthly thermal amplitude of the reference and experimental cubicle

Month	Reference cubicle		Experimental cubicle		(ΔT_r) Thermal amplitude of Reference cubicle ($T_{max,r}$- $T_{min,r}$)	(ΔT_e) Thermal amplitude of experimental cubicle ($T_{max,e}$- $T_{min,e}$)	(α) %Reduction in thermal amplitude (ΔT_r- ΔT_e)/ΔT_r
	$T_{max,r}$	$T_{min,r}$	$T_{max,e}$	$T_{min,e}$			
January	18.7	10.4	18.4	11	8.3	7.4	10.8%
February	23.5	12.8	22.9	12.2	10.7	10.7	0%
March	40.7	22.7	37.2	22.7	18	14.5	19.44%
April	39.1	28.8	36	28.6	10.8	7.4	31.48%
May	41.3	28	38	29.3	13.3	8.7	34.5%
June	41.6	30.7	38	31	10.9	7	35.77
July	41.6	30.7	37.9	32.6	10.9	5.3	51.37
August	42.3	30.4	38	31	11.9	7	41.17
September	41	29.8	37.5	30.4	11.2	7.1	36.60
October	39.3	28.6	37.7	29.1	10.7	8.6	19.62
November	39.3	26.1	37.1	26.6	13.2	10.5	20.45
December	27.6	19.4	27.4	19	8.2	8.4	-2.43

Two important factors i.e. Time lag (ϕ) and Decrement factor (f) play a critical role in improving the indoor thermal performance of the buildings (283). Time lag and decrement factor are the important thermal inertia parameters for the analysis and interpretation of the heat storage capabilities of the building envelopes. The time it takes for the heat wave to propagate from the outer surface towards the inner surface of the building is called as 'time lag' and the decreasing ratio of its amplitude during this process is termed as 'decrement factor' (284). Thus it becomes crucial to evaluate these two parameters for a building to provide a measure of developed indoor thermal stability and possibilities of minimizing the energy consumption for space cooling. In the tropical and hot equatorial climate building

envelope with high time lags and small decrement factor, improves the indoor thermal comfort level.

For any building structure, these two factors depend on thermo-physical properties and the thickness of the walls (285). It is necessary to design the building envelope in such a way that a high time lag and low decrement factor is achieved so that the high fluctuations in the outdoor temperature must not propagate inside and results in good thermal stability. The time lag and decrement factor for a wall are usually expressed as followed (286).

$$\text{Time lag } (\phi) = t_{T_{i,max}} - t_{T_{o,max}} \qquad (4.1)$$

$$\text{Decrement factor} = \frac{T_{i,max} - T_{i,min}}{T_{o,max} - T_{o,min}} \qquad (4.2)$$

Where, $t_{T_{i,max}}$ and $t_{T_{o,max}}$ are the time when inside and outside temperature are maximum and $T_{i,max}$, $T_{i,min}$, $T_{o,max}$, and $T_{o,min}$ are the maximum and minimum indoor and outdoor temperature. In this study, the indoor thermal performance of the experimental cubicle in comparison to the reference cubicle has been analyzed therefore; the time lag achieved by the experimental cubicle compared to the reference cubicle is evaluated. Figure 4.25 depicts the monthly time delay of the experimental cubicle in reaching the peak indoor ambient temperature mark in comparison to reference cubicle and Figure 4.26 shows the monthly decrement factor of reference cubicle and experimental cubicle. It has been observed that a variation of minimum 60 min to a maximum of 180 min in time lag from March to October is achieved by the experimental cubicle. The month of May and July has shown the maximum time lag of 180 min. However, the months of January, February, November and December of the experimental cubicle have shown zero time-lag compare to the reference cubicle. An annual average time lag of 97.5 min was obtained by the experimental cubicle.

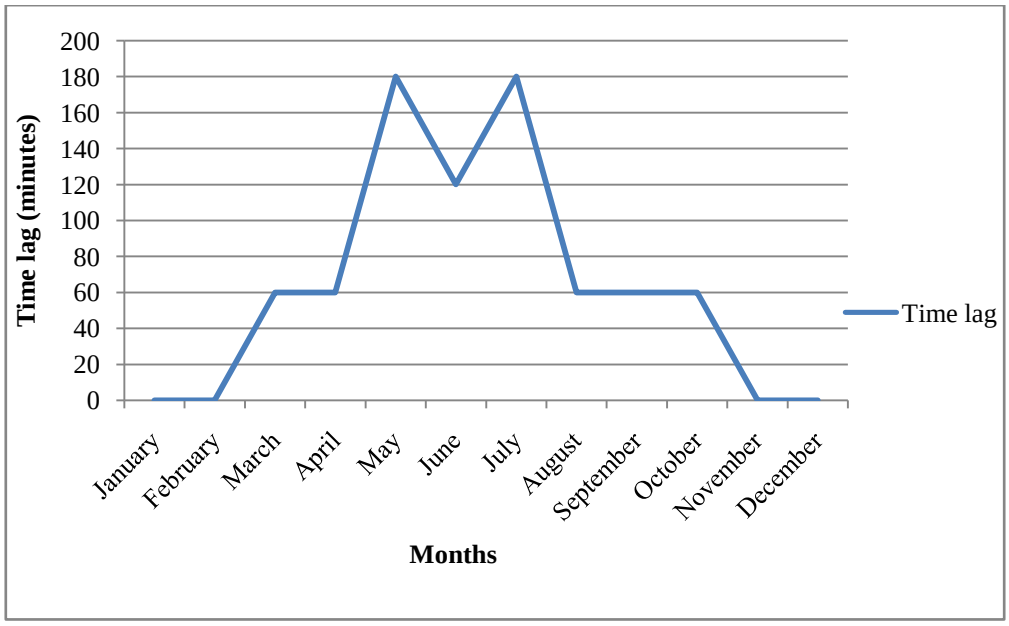

Figure 4.26 Monthly time lag of experimental cubicle in comparison to the reference cubicle

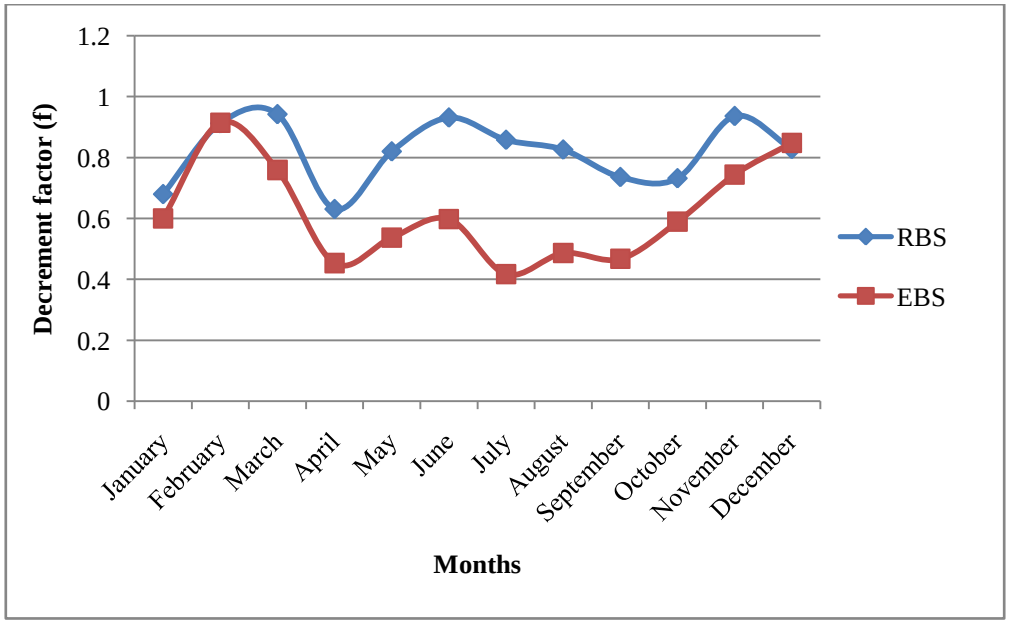

Figure 4.27 Monthly decrement factor of the reference and experimental cubicle

The analysis of the decrement factor shows that the experimental cubicle has obtained a lower value of decrement factor from March to November compare to the reference cubicle. For the month of January, February and December the decrement factor of both the cubicle remains almost equal. The annual average decrement factor of 0.61 and 0.81 was evaluated for the experimental and reference cubicle respectively. Thus an annual average reduction of 24.69% in the decrement factor was obtained for the experimental cubicle. This will reduce the summer overheating of the experimental cubicle more effectively than the reference cubicle. These results suggest that the experimental cubicle has the potential of increasing the time delay and reducing the decrement factor.

4.2.2 Annual cost savings in peak heat flux

Heat flux is defined as the amount of heat transfer from per unit of the area in per unit time. The heat flux greatly influences the thermal performance of the building enclosure and hence, affects the heating/cooling load requirements. For the analysis of the heat flux of both the BS, heat flux sensors HFP01 from hukseflux were used. The sensors were placed on each wall and on the roof of both the BS. To evaluate the total peak value of heat transfer of both the cubicles, the peak heat fluxes of all the walls and roof was added. The analysis of the monitored peak heat flux data suggest that the experimental cubicle has shown a percentage reduction of 27.14 %, 26.15%, 26.75%, 29.09%, 25.05%, 26.53%, 25.41%, and 14.77% for the month of March, April, May, June, July, August, September and October respectively in comparison to the reference cubicle. Whereas, almost negligible reduction in the peak heat flux was observed for the month of January, February, November and December of the experimental cubicle compared to the reference cubicle. The maximum and minimum reduction in the peak heat flux of 29.09% and 0.15 % was observed for the month

of June and December respectively. This shows that the walls and the roof of the experimental cubicle are sufficiently insulated against the heat transfer from outdoor to indoor in comparison to the reference cubicle. The sum of peak heat fluxes from all the orientation represents the peak space cooling load required for the cubicle, if radiation losses were neglected. In this study, heat entered through all the orientation was considered for the calculation of the peak cooling load. It must be noted that the heat flux through the walls of both the cubicles would fluctuate and reaches the peak at different times of the day. The difference between the peak heat fluxes of the reference and experimental cubicle represents the reduction in the peak heat flux. If radiation losses are assumed to be neglected then the peak heat flux value will represent the peak cooling load of both the BS. Assuming the unit price of electricity in India to be 5.5 rupees in the year 2019. Therefore, per day cost-saving in the peak load will be evaluated as:

Cost saving (Per day) = Reduction in the peak heat flux × unit price of the electricity × 24 hours. (4.3)

Putting the measured value in the equation (4.3), the cost saving of every month will be evaluated and is shown in Table 4.5. From Table 4.5 it is clear that because of the presence of the MPCM in the building envelope, the experimental cubicle recorded low peak heat flux in comparison to the reference cubicle. Consequently, there will be a reduction in the peak cooling load requirement which results in cost savings. The savings in energy for the peak cooling load of experimental cubicle varies from 0.01 Rupees/kWh/m^2/day to 2.78 Rupees/kWh/m^2/day. The results suggest that most of the cost savings occur in the months of the summer season when the global solar irradiance lies between 6.04 kWh to 7.82 kWh. Table 4.6 compares the results of present study with similar previous published studies.

Table 4.5 Comparison of the peak heat fluxes of the RBS and EBS and corresponding cost savings

Months	Reference cubicle peak heat flux (W/m^2)	Experimental cubicle peak heat flux (W/m^2)	Percentage reduction	Global solar irradiance (kWh)	Cost saving per day (Rupees/kWh/m^2)
January	32.86	32.42	1.33	3.22	0.05
February	36.55	35.89	1.80	3.92	0.08
March	60.9	44.37	27.14	6.30	2.06
April	65.76	48.56	26.15	7.82	2.15
May	71.32	52.24	26.75	7.82	2.38
June	76.54	54.27	29.09	6.04	2.78
July	80.47	60.31	25.05	6.88	2.52
August	74.1	54.44	26.53	6.55	2.45
September	63.83	47.61	25.41	6.15	2.02
October	51.04	43.5	14.77	6.15	0.94
November	40.71	38.94	4.34	4.09	0.22
December	31.27	31.22	0.15	3.22	0.01
Avg.	**57.11**	**45.31**	**17.37**	**5.68**	**1.47**

Table 4.6 Comparison of experimental result with previous published literature

PCM	Container type/material	Heat flux reduction	Thermal amplitude	Peak Temperature reduction	Time lag	Energy savings	Ref.
Paraffin wax	Metal steel	-	50 % - 80 %	-	3 h	-	(67)
RT18	Steel	-	5 -10 °C	-	3 h	0.52 kWh/m^2	(117)
SP29 and RT18	Aluminum panels	-	28.8 – 67.8%	4.28 – 7.7 °C	-	-	(68)
Capric acid and 1-dodecanol	Aluminum sheet	-	-	1 – 2.3 °C	2.1 h to 3 h	-	(69)
RT28HC	Aluminum	40 - 45%	18 % - 22 %	6 – 11 %	45 min	-	(118)
RT27	Copper pipes	22.5-36.5%	-	-	89- 116 min	27.4-51.2Wh/m^2	(72)
Hydrated salt	Polymer pouches	29.7-51.3%	-	-	2.3-6.3h	-	(71)
Paraffin wax	Aluminum	-	-	1.2 – 3.3 °C	-	2.114 kW/m^3	(74)
OM37	**Aluminum pipes**	**38.76%**	**40.67-59.79%**	**3.1-3.7 °C**	**60-120 min**	**0.226 kWh**	**This study**

4.3 THERMAL ENERGY STORAGE PERFORMANCE

The thermal energy storage performance of the PCM required to improve the latent heat storage capacity of the buildings was investigated in this section. As the thermal conductivity of the PCM is low, it reduces the heat transfer rate and adversely affects the charging and discharging rate of the PCM. Thus, to improve the heat transfer rate of the PCM, series of composite PCM was prepared using highly conductive expanded graphite (EG) nanoparticle and highly porous expanded vermiculite (EV) clay. Additionally, the presence of highly porous EV prevents the leakage of the PCM when embedded in the building element. Following properties affecting thermal energy storage performance of the PCM are investigated and discussed in this section.

1. Thermal energy storage
2. Thermal transient response
3. Thermal decomposition
4. Thermal reliability
5. Thermal conductivity
6. Leakage-proof performance

4.3.1 Thermal energy storage

The DSC testing was used to evaluate the latent heat storage capacity and phase change temperature of the ss-CPCM. The theoretical calculated latent heat storage capacity of ss-CPCMs can be evaluated from equation (1).

$$\Delta H_{ss\text{-}CPCM} = \eta \times \Delta H_{PCM} \qquad (1)$$

In equation (1), $\Delta H_{ss\text{-}CPCM}$ is calculated latent heat storage capacity of ss-CPCMs, η is the weight fraction of PCM in ss-CPCM, and ΔH_{PCM} is the latent heat capacity of the PCM measured by the DSC. Figure 4.28 shows the DSC testing of PCM with thermal cycle and without thermal cycle.

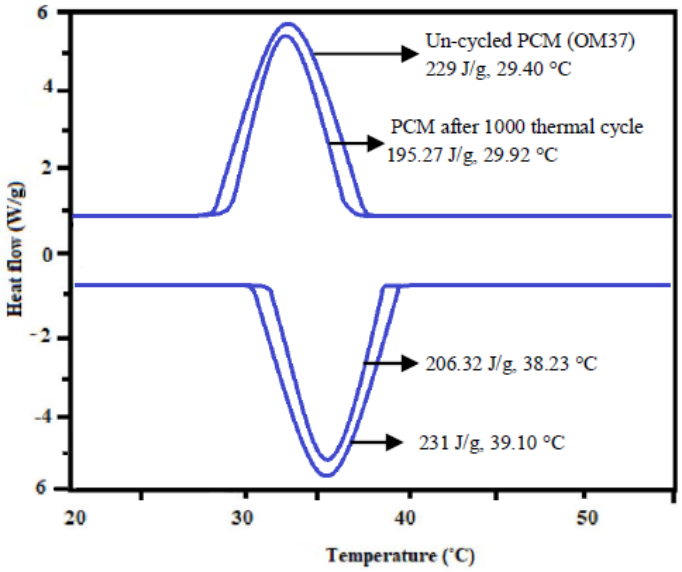

Figure 4.28 DSC testing results of PCM (OM37)

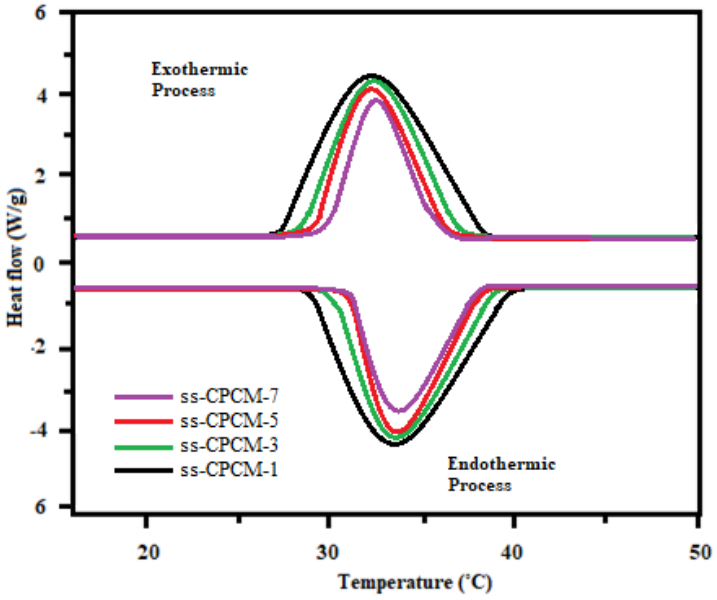

Figure 4.29 DSC testing results of ss-CPCM without thermal cycles

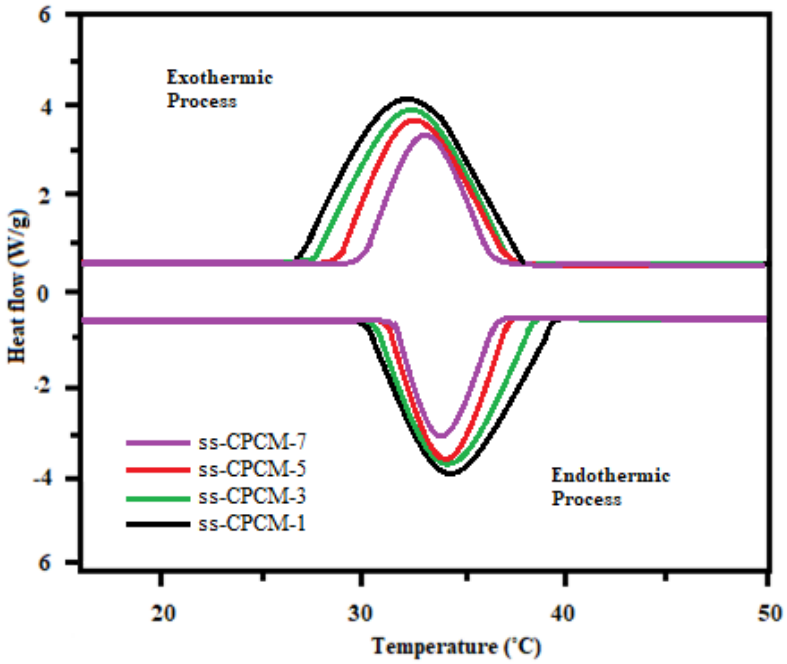

Figure 4.30 DSC testing results of ss-CPCM after 1000 thermal cycles

The PCM shows one endothermic peak and one exothermic peak. Similarly, It has been seen from the Figure 4.29 and Figure 4.30 that ss-CPCM exhibits regular endothermic and exothermic peaks for all the samples. The DSC curves of ss-CPCM-1, 3, 5, and 7 overlapped each other with little deviations, suggesting that all ss-CPCM exhibits similar phase change and thermal energy storage behavior. The ss-CPCM-1, 3, 5, and 7 without thermal cycles completely melts at 40.61 °C, 39.12 °C, 38.83 °C and 37.41 °C respectively. The ss-CPCM-1, 3, 5, and 7 after 1000 thermal cycles completely melts at 40.09 °C, 38.41 °C, 37.22 °C, 37.00 °C respectively. Similarly, the ss-CPCM-1, 3, 5, 7 without thermal cycles freezes at 28.23 °C, 29.54 °C, 30.87 °C, 31.21 °C respectively and ss-CPCM-1, 3, 5, 7 after 1000 thermal cycles freezes at 28.86 °C, 29.90 °C, 31.04 °C, 31.68 °C respectively. The deviation of phase change temperature of the ss-CPCM after 1000 thermal cycles was almost

negligible, suggesting higher thermal stability as a thermal energy storage material. Also, phase change temperatures of ss-CPCMs were not affected by the loading of EG. The latent heat of melting and freezing of ss-CPCM-1is 114.23 J/g and 112.82 J/g, ss-CPCM-3 is 111.56 J/g and 108.22 J/g, ss-CPCM-5 is 105.08 J/g and 102.56 J/g, ss-CPCM-7 is 99.32 J/g and 87.62 J/g respectively. The latent heat capacity of the ss-CPCM reduced in comparison to PCM because of increase in the content of EV and EG in the ss-CPCM and EV and EG does not participate in phase transition therefore, they don't store thermal energy in latent form. Additionally, the increase in mass fraction of EVM and EG, and reduction in mass fraction of PCM restricts the motions of PCM particles during crystallization due to strong interactions of EVM, EG, and PCM was also reduced in ss-CPCMs.

Table 4.7 DSC analysis of PCM and ss-CPCM

PCM	Melting Temperature(°C)	Freezing Temperature (°C)	Latent heat of melting, H_m (J/g)	Calculated latent heat of melting, H_c	Latent heat of freezing, H_s (J/g)	Calculated latent heat of melting, H_c
	Uncycled PCM composite					
PCM	39.10(±0.09)	29.40(±0.13)	231(±0.47)	231	229(±0.39)	229
ss-CPCM-1	40.61(±0.18)	28.23(±0.27)	114.23(±1.18)	115.5	112.82(±1.53)	114.5
ss-CPCM-3	39.12(±0.11)	29.54(±0.18)	111.56(±0.64)	112.03	108.22(±1.41)	111.06
ss-CPCM-5	38.83(±0.08)	30.87(±0.11)	105.08(±1.03)	109.72	102.56(±0.75)	108.77
ss-CPCM-7	37.41(±0.07)	31.21(±0.08)	99.32(±0.71)	107.41	97.62(±0.84)	106.48
	After 1000 thermal cycle					
PCM	38.23(±0.19)	29.92(±0.15)	206.32(±0.14)	206.32	195.27(±0.06)	195.27
ss-CPCM-1	40.09(±0.17)	28.86(±0.12)	102.48(±1.84)	103.16	96.71(±1.70)	97.63
ss-CPCM-3	38.41(±0.12)	29.90(±0.10)	98.60(±01.07)	100.06	93.03(±1.68)	94.70
ss-CPCM-5	37.22(±0.07)	31.04(±0.12)	91.71(±0.66)	98.02	90.62(±0.71)	92.75
ss-CPCM-7	37.00(±0.08)	31.68(±0.08)	88.44(±0.47)	95.93	86.02(±0.37)	90.80

A reduction of 50.54%, 51.70%, 54.51%, and 57.0% in the latent heat storage capacity of ss-CPCM-1, 3, 5, and 7 respectively was observed in comparison to OM 37 PCM. Table 4.6 shows the DSC data of ss-CPCM with and without thermal cycles. Table 4.7 shows the measured phase change temperatures and latent heat values of ss-CPCMs. It can be seen that the measured values of latent heat thermal energy storage of all the ss-CPCM samples are in good agreement with calculated latent heat value.

4.3.2 Thermal stability analysis

The thermal stability analysis was done by TGA technique. In this the temperature of the tested sample rises slowly from 20 °C to 400 °C at a rate of 10 °C/min. The corresponding loss of wt% of the sample with the increase in temperature is plotted and analyzed for thermal decomposition. Thermal decomposition (%) of the PCM and ss-CPCM in different temperature ranges was shown in Table 4.8.

Table 4.8 Thermal decomposition (%) of the PCM and ss-CPCM in different temperature ranges

Sample	20-150 °C	150-300 °C	300-400°C
	Uncycled		
PCM	0	51.24	48.76
ss-CPCM-1	0	46.53	6.27
ss-CPCM-3	0	40.04	10.66
ss-CPCM-5	0	35.87	13.73
ss-CPCM-7	0	29.34	19.6
	1000 cycles		
PCM	0	71.30	28.70
ss-CPCM-1	0	48.63	5.47
ss-CPCM-3	0	43.41	8.99
ss-CPCM-5	0	38.76	11.54
ss-CPCM-7	0	32.23	16.87

The PCM starts losing its weight at 170 °C and completely loss its weight until 370 °C as shown in Figure 4.31. However, the PCM doesn't show any weight loss in between 20 °C to 170 °C. The ss-CPCM samples show no loss of weight in between 20 °C to 180 °C. The weight loss of ss-CPCM starts after 180 °C and continue gradually until 250 °C. However, a sudden weight loss of all the ss-CPCM was observed after 250 °C, which continues until 330 °C. A weight loss of 52.8%, 50.7%, 49.6%, and 48.5% was measured for ss-CPCM-1, 3, 5, and 7. The PCM content of all the ss-CPCM samples was vaporized in between the temperature range of 180 °C and 320 °C. However, small amount of weight loss (maximum of 2.8%) of EV/EG was also observed along with PCM in ss-CPCM. From 330 °C to 400 °C the sample doesn't show any degradation in weight. Similar behavior of thermal stability was also shown by ss-CPCM after 1000 thermal cycles as shown in Figure 4.32. No sign of weight loss was observed till 165 °C for all the samples of ss-CPCM. A weight loss of 49.1%, 50.3%, 52.4%, and 54.1% was observed for ss-CPCM-1, 3, 5, and 7 respectively till 320 °C. A major portion of weight loss in all the ss-CPCM samples was of PCM. The deviation in weight loss with respect to temperature, of ss-CPCM with thermal cycle in comparison to ss-CPCM without thermal cycles, is because of the physical deterioration occurring due to 1000 melting-freezing cycles. These results suggest that the ss-CPCM is thermally stable due there high durability in a temperature range which is mostly required in thermal energy storage applications in buildings.

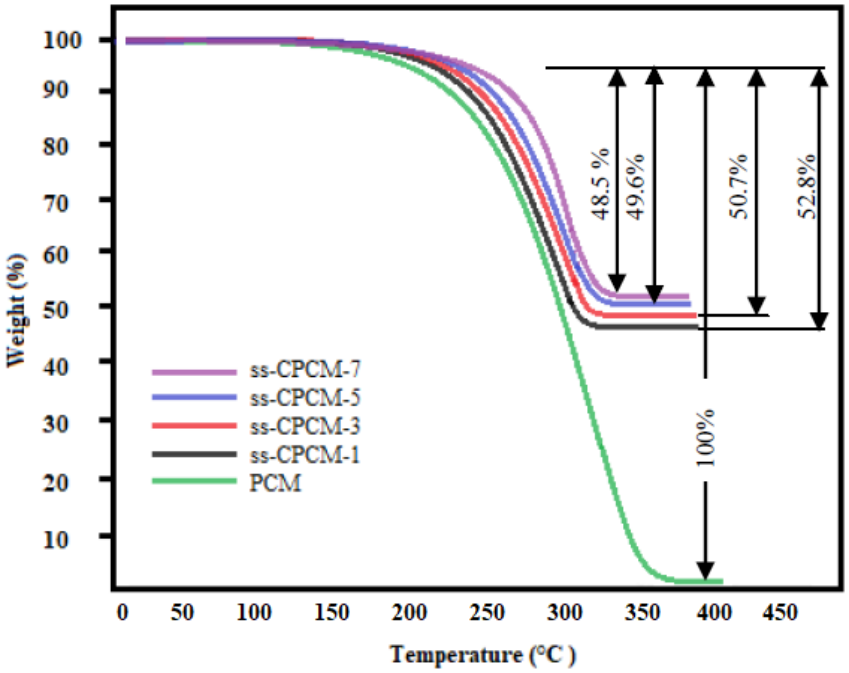

Figure 4.31 TGA results of ss-CPCM

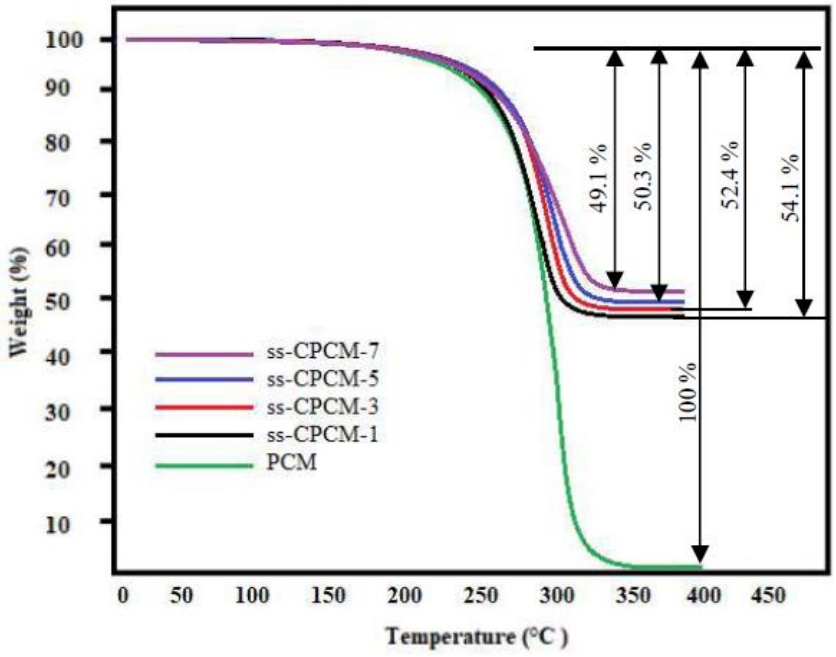

Figure 4.32 TGA results of ss-CPCM after 1000 thermal cycles

4.3.3 Transient thermal response

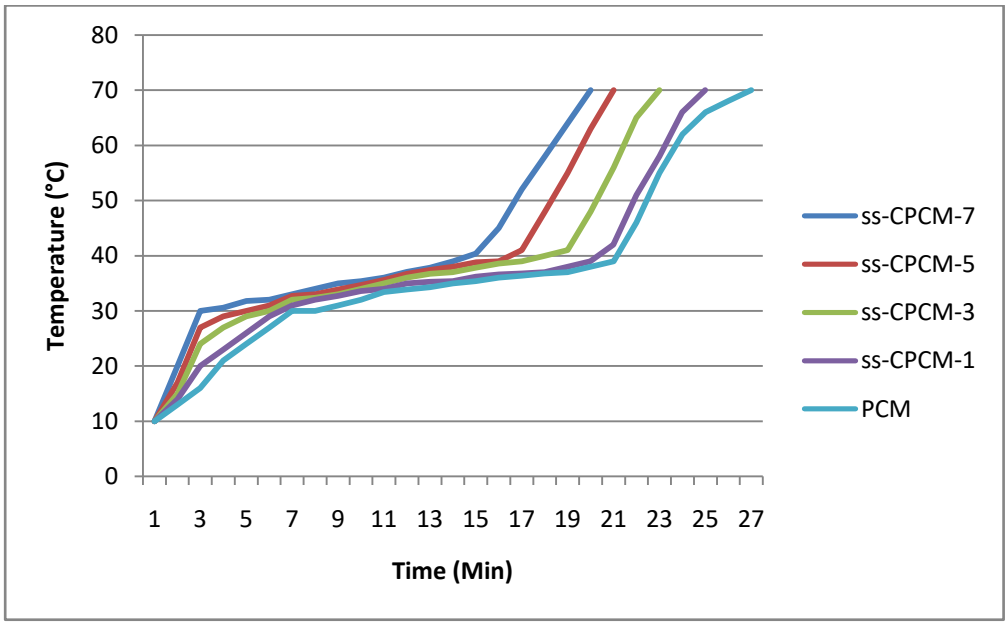

Figure 4.33 Melting curve of ss-CPCM

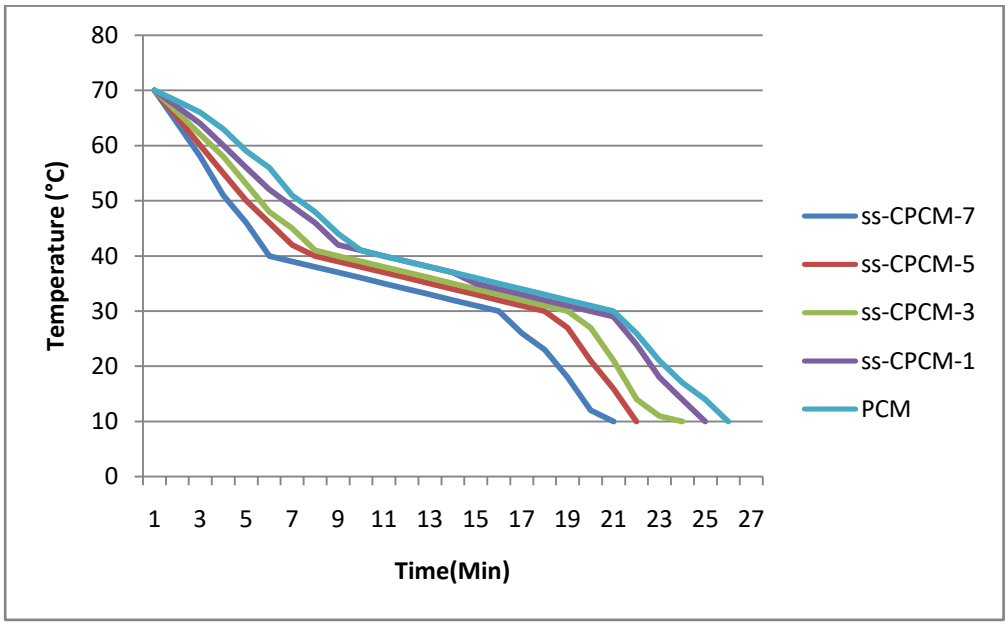

Figure 4.34 Freezing curve of ss-CPCM

The melting cycle and freezing cycle of ss-CPCM defines how well it response to the change in temperature. Figure 4.33 and Figure 4.34 shows the melting and freezing curve of ss-CPCM respectively in the temperature range of 10° C to 70° C and for 25 minutes. The melting curve can be divided into three different zones viz. non-melting zone, phase transformation zone and melted zone. In non- melting zone the temperature of ss-CPCM samples rises sharply but no phase change occurs. ss-CPCM-1, 3, 5, and 7 has taken 7 min, 5 min, 4min and 3 min respectively to reach the temperature mark of 30°C. However, the pure PCM has taken a maximum time of 9 min to reach the temperature mark of 30°C. This shows that due to the addition of EG the time taken to reach the melting temperature mark was reduced because of increase in heat transfer rate. The second zone is phase transformation zone where ss-CPCM undergoes the solid-liquid phase transformation. ss-CPCM-1, 3, 5, and 7 has taken 20 min, 17 min, 16 min, and 14 min respectively to reach the complete molten form. This suggests that, increasing the content of EG in the composite will enhance the heat transfer rate and thereby reduces the time to reach the melting point mark. The third zone is the melted zone where temperature of ss-CPCM in liquid form rises suddenly. Here the heat transfer occurs due to natural convection supported by the thermal conductivity. The ss-CPCM-7 has taken least time to reach the 70 °C mark followed by ss-CPCM-5, 3, and 1. Thus, ss-CPCM-7 has shown 25.9% faster heating rate in comparison to pure PCM. Similarly, ss-CPCM-5, ss-CPCM-3, ss-CPCM-1 has recorded 22.2%, 14.8% and 7.3% faster heating rate respectively in comparison to PCM.

The freezing curve of ss-CPCM can also be divided into three different zones. Zone one is the melting zone, zone two is the liquid-solid phase change zone and zone three is the freezing zone. In zone one, the temperature of ss-CPCM falls suddenly without any phase

change. EG loaded ss-CPCM shows a faster rate of temperature reduction in comparison to ss-CPCM-1 and pure PCM. The ss-CPCM-1, 3, 5, and 7 reaches the phase transition temperature range in 11 min, 9 min, 8 min, and 6 min respectively. In zone second, the phase transition from liquid to solid occurs and marks the beginning of crystal formation. The ss-CPCM solidifies and the temperature reaches to freezing point. This zone signifies with the large amount of heat dissipation in the temperature range of 40 °C to 30 °C. The fall in temperature in this zone is gradually however, ss-CPCM loaded with EG shows faster reduction in temperature in comparison to ss-CPCM-1 and pure PCM. The time taken to reach the freezing point by ss-CPCM-1, 3, 5, and 7 are 20 min, 19 min, 18 min, and 16 min respectively. Pure PCM has taken 21 min to reach freezing point from 70 °C temperature. The third and the last zone is the freezing zone where temperature falls further from freezing temperature to 10 °C. This zone shows sudden fall in the temperature with no heat loss. The ss-CPCM-7 has taken least time of 21 min to reach the temperature of 10 °C followed by ss-CPCM-5 with 22 min, ss-CPCM-3 with 24 min, ss-CPCM-1 with 25 min, and pure PCM with 26 min. Thus, ss-CPCM-1, 3, 5, and 7 has shown 3.7%, 7.6%, 15.3% and 19.2% faster freezing than PCM.

4.3.4 Thermal conductivity

Thermal conductivity is an important characteristic of inorganic PCM while considering them for thermal energy storage in buildings. Thermal conductivity is defined as rate of heat transfer per unit area in per unit time. High thermal conductivity of the PCM will ensure high rate of heat transfer resulting in quick charging and discharging of the PCM. The thermal conductivity was measured using TPS sensor. The results are average of five reading of each samples of ss-CPCM. Table 4.9 shows the details of thermal

conductivity recorded for ss-CPCM and percentage change in it in comparison to PCM. The values shown in bracket are thermal conductivity after 1000 thermal cycles. The PCM has thermal conductivity of 0.145 W/mK. An 11.7 % of reduction in the thermal conductivity of ss-CPCM-1 was recorded compare to the PCM. ss-CPCM-1 has thermal conductivity of 0.128 W/mK. The reduction in the thermal conductivity is due to the presence of EV, because EV exhibits a low thermal conductivity of 0.118 W/mK. The thermal conductivity of ss-CPCM-3, 5, and 7 has shown a improvement of 33.1 %, 79.3 %, and 114.4 % respectively in comparison to the PCM. The rise in the thermal conductivity is because of the presence of EG in ss-CPCM. Table 4.10 shows a comparative analysis of thermal properties of the prepared ss-CPCM with the previously published literature on similar ss-CPCMs. It could be noted that the thermal properties of the prepared ss-CPCM are competitive with that of earlier conducted studies.

Table 4.9 Thermal conductivity measurement of ss-CPCM with corresponding percentage improvement

S.No.	Sample	EG Weight %	Thermal conductivity (W/mk)	Improvement (%)
1	PCM	0	0.145 (0.142)	0 (0)
2	ss-CPCM-1	0	0.128 (0.122)	-11.7 (-14.0)
3	ss-CPCM-3	3.0	0.193 (0.187)	33.1 (31.6)
4	ss-CPCM-5	5.0	0.260 (0.254)	79.3 (78.8)
5	ss-CPCM-7	7.0	0.311 (0.302)	114.4 (112.6)

Values in brackets are the values after 1000 thermal cycles

Table 4.10 Comparison of thermal properties of PCM/EV/AO ss-CPCM of this study with previously published studies on similar ss-CPCMs.

ss-CPCM	Thermal conductivity	Latent heat storage of melting	Latent heat storage of freezing	Melting temperature	Reference
Octadecane/EV	0.2310	142.0	126.5		(170)
Salt hydrate/EV	0.192	110.3	79.6	23.98	(42)
Stearic acid/Modified EV	0.58	146.8	141.7	65.9	(192)
Lauric-Myristic-Stearic acid/EV/Al_2O_3	0.671	113.7	108.5	28.6	(58)
Capric-Myristic-Stearic acid/acid treated EV/carbon composite	0.667	86.4	80.4	22.92	(197)
Stearic acid/EV/Carbon	0.52	134.31	135.94	67.12	(287)
Polyethylene glycol/3.29 wt% silicon carbide nanowire/EV	0.53	64.93	60.48	51.87	(288)
48.5 wt% PCM/48.5 wt% EV/3.0 wt% AO	0.193	147.81	140.22	39.12	This work
47.5 wt% PCM/47.5 wt% EV/5.0 wt% AO	0.260	116.08	108.56	38.83	This work
46.5 wt% PCM/46.5 wt% EV/7.0 wt% AO	0.311	91.32	85.62	37.41	This work

4.3.5 Leakage-proof performance of ss-CPCM

Thermal energy storage applications of PCM requires leakage-proof performance. To evaluate the leakage-proof performance of ss-CPCM, the samples of ss-CPCM are heated at 30°C for 10 minutes. After 10 minutes the temperature was further increased to 40°C for 30 minutes and the results are shown in Figure 4.35. Initially, when the samples were heated at 30°C, the PCM starts melting with obvious leakage on the qualitative filter paper. All ss-CPCM samples, however, retains the original shape without showing any sign of leakage. When the temperature was further increased and maintained at 40°C for 30 minutes, the PCM completely melts to liquid. The ss-CPCM-1 also shows leakage of PCM which spreads out in liquid form in the qualitative filter paper. The leakage from ss-CPCM-1 can be attributed to higher loading of PCM (50 wt%) in the sample. However, no leakage was observed in ss-CPCM-3, ss-CPCM-5, and ss-CPCM-7 samples, which suggest that ss-

CPCM have extraordinary leakage proof property. The extraordinary leakage proof performance of the ss-CPCM is because of the presence of EV. The closed-cell structure of the pores exerts enough capillary force to retain the PCM during phase transition process. It has been view that for ss-CPCM, the lower the content of the PCM, the better the leakage proof performance.

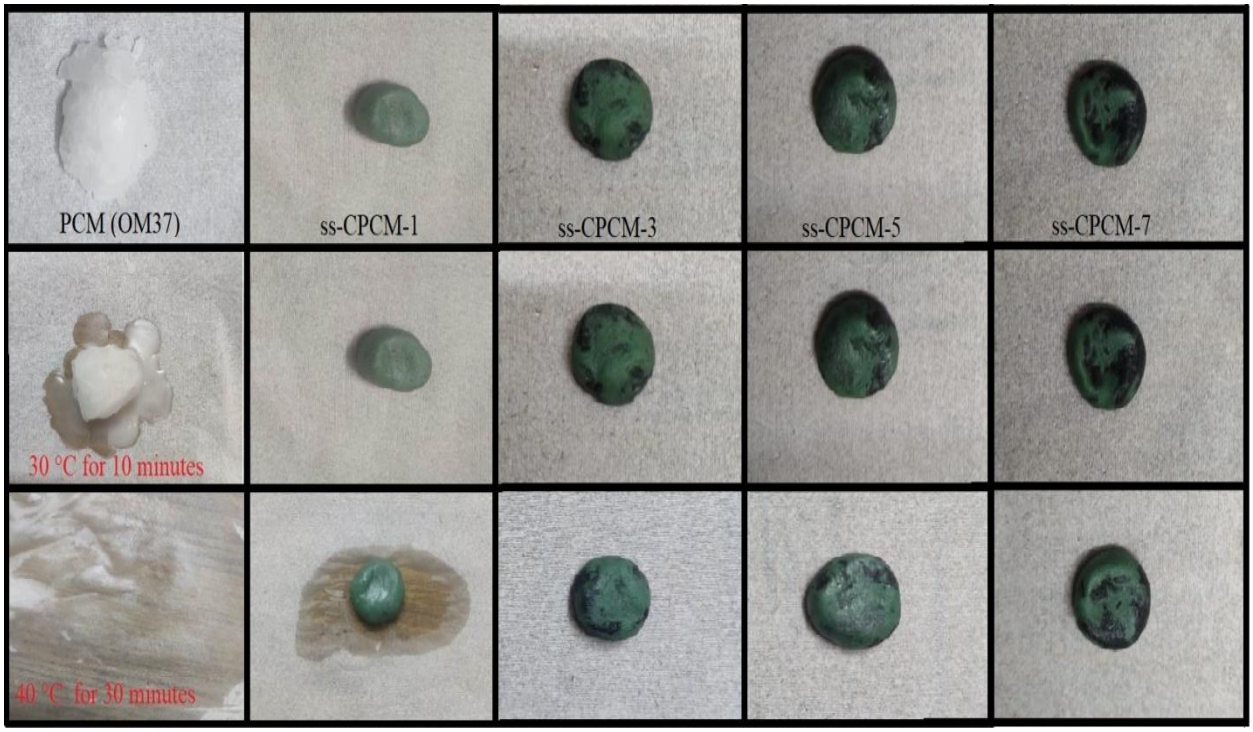

Figure 4.35 Leakage proof performance of ss-CPCM at 30 °C for 10 minutes and at 40 °C for 30 minutes